Passive Multiuser Teleoperation of a Multirobot System With Connectivity-Preserving Containment

Yuan Yang, *Member, IEEE*, Daniela Constantinescu, *Member, IEEE*, and Yang Shi, *Fellow, IEEE*

***Abstract*—A remote multirobot system (RMRS) outfitted with wireless sensors for large-scale data collection may need to be tele-driven by several human users simultaneously. The long distances between the users' local robots and the RMRS can inject time-varying delays in their communications. This article enables such multiuser teleoperation of an RMRS through a control strategy that robustly synchronizes an RMRS with tree topology and proximity-limited one-hop communications among its robots, enables multiple users to tele-guide the RMRS and to feel the actions of the other users over time-delayed communications between the users' local robots and the RMRS, and contains the RMRS to the stationary convex hull spanned by the local robots of all users in the steady state. A control design constrained by the connectivity of the RMRS and by the passivity of the teleoperator guarantees effective coordination, safe teleoperation, and steady-state containment. The design is a dynamic feedforward–feedback passivation strategy facilitated by a suitable decomposition of the teleoperator into interconnected subsystems. The analysis of the storage functions, and thus of the input–output relations, of all subsystems and their interconnections proves the properties of the design. Comparative experiments in a teleoperation testbed with four local and ten remote robots validate its practical efficacy.**

***Index Terms*—Bilateral teleoperation, connectivity, containment, multirobot systems, passivity.**

I. Introduction

THE potential of deploying large-scale robotic networks in promising applications, such as the exploration of unknown environments [1], surveillance and reconnaissance [2], and cooperative transportation [3], has recently led to significant interest in the control of multirobot systems [4]. Despite their flexibility and robustness to failures, fully autonomous multirobot systems lack high-level cognitive-based decision making and cannot cope with complex tasks in uncertain or dynamic environments. Human intelligence is often preferred and even indispensable for handling unpredictability in the real world [5]. In this context, bilateral teleoperation can enable human users, assisted by haptic perception, to intervene in the control of remote multirobot systems (RMRSs).

For the teleoperation of tight formations of RMRSs, a centralized passive strategy decomposes the dynamics of holonomic [6] and nonholonomic [7] RMRSs into a locked system and a shape system and cancels their interference. The method further permits to coordinate and tele-drive two mobile robots using a single first-person view camera [8]. Alternatively, proportional–derivative control couples the local robot of a single user to all robots of the RMRS [9]. For the teleoperation of flexible formations of RMRSs, distributed controls with arbitrary link additions and deletions [10] use energy tanks [11] to passivate the RMRS and use feedback r-passivity [12] to coordinate a leader robot of the RMRS with a kinematically dissimilar local robot of the user. Extensions address communication delays through a two-layer control architecture [13] and optimize the tracking performance via dynamic leader selection [14], [15]. A virtual structure enables the teleoperation of an end-to-end aerial robotic swarm with switching formations but without force feedback [16].

Other research pertinent to bilateral teleoperation of RMRSs focuses on the decentralized control of the RMRS or on the interconnections between the users' local robots and the RMRS. Decentralized control leads to the teleoperation of an RMRS formation with only bearing measurements [17] and to the estimation of the human command and task functions by consensus algorithms at the RMRS [18]. Force feedback shaped through passivity-constrained quadratic programming improves the haptic interaction [19]. A concept of trust [20] augmented with self-confidence [21] allocates autonomy and selects a leader [22] during the teleguidance of an RMRS.

Cooperative teleoperation [23] and haptic interaction [24] inspire the multiuser multirobot teleoperation problem in this article. The cooperative teleoperation designs reviewed in [25] and recently studied in [26] and [27] aim to synchronize the local robots of all the users with all the robots of the RMRS by transmitting/receiving messages to/from a shared network. In cooperative haptic interaction [24], the local proxies of the virtual object are synchronized with no proximity constraints. In contrast, this article focuses on a distributed robotic sensor network teleoperated by multiple users for large-scale data collection in unknown environments. In the system, 1) every remote robot exchanges information with other remote robots in a tree communication network, and 2) each human operator

Manuscript received December 10, 2020; revised March 20, 2021; accepted May 10, 2021. Date of publication June 23, 2021; date of current version February 8, 2022. This work was supported by the Natural Sciences and Engineering Research Council of Canada (NSERC) under Grant 34771 and Grant 34199. This article was recommended for publication by Associate Editor A. Prorok and Editor P. Robuffo Giordano upon evaluation of the reviewers' comments. *(Corresponding author: Daniela Constantinescu.)*

Yuan Yang is with the Department of Electrical Engineering, Polytechnique Montréal, Montréal, QC H3T 1J4, Canada (e-mail: yuan.yang@polymtl.ca).

Daniela Constantinescu and Yang Shi are with the Department of Mechanical Engineering, University of Victoria, Victoria, BC V8W 2Y2, Canada (e-mail: danielac@uvic.ca; yshi@uvic.ca).

This article has supplementary material provided by the authors and color versions of one or more figures available at https://doi.org/10.1109/TRO.2021.3086685.

Digital Object Identifier 10.1109/TRO.2021.3086685

manipulates their local robot to command a unique (leader) remote robot of the RMRS. Thus, the users interact with their peers implicitly over a distributed RMRS. Most importantly, the proposed control accommodates the proximity constraints of wireless communications among the remote robots, enables bilateral teleoperation over time-delayed communications between the local robots of the users and the RMRS, and guarantees the containment of the RMRS when the users hold their local robots stationary.

In summary, the proposed controller for multiuser teleoperation of distributed RMRSs guarantees the following:

1) the connectivity of the RMRS and its robust coordination with the local robots of the users;
2) the passivity of the bilateral teleoperator with time-delayed communications between the local robots of the users and the RMRS;
3) the convergence of the RMRS to the convex hull spanned by the stationary local robots.

II. Related Work

The key contribution of this article is the distributed containment control, in the framework of multiuser teleoperation, of an RMRS subject to two constraints: the connectivity of the RMRS and the passivity of the bilateral teleoperator. Hence, this section reviews three areas of directly related work: connectivity preservation of multirobot systems, passive bilateral teleoperation, and connectivity-preserving swarm teleoperation.

A. Connectivity Preservation of Multirobot Systems

Network connectivity is fundamental in decentralized [28] and distributed [29] control of coordinated multirobot systems. Early research preserves the local connectivity of multirobot systems: it maintains all initial communication links by connecting the robots with gradient-based gains derived from an unbounded potential [30]. For increased flexibility, later work ensures the global connectivity of multirobot systems: it creates and deletes links without disconnecting the network. For first-order multirobot systems, hybrid control combines discrete-time decision-making mechanisms over the network, such as market-based auction [31] and event-driven prediction [32], [33], with continuous-time potential-based local actuation. A supergradient policy maximizes the algebraic connectivity [34], and a decentralized power iteration estimates it [35].

A robust algebraic connectivity estimation technique and a gradient-based control derived from an unbounded potential maintain connectivity in the presence of extra bounded control terms [36]. The concept of critical robots reduces both the negative impact on the major task and the control effort of the robust connectivity-preserving approach [37]. The interference between global connectivity maintenance and other collective control objectives under limited actuation is clarified in [38]. Two-hop communications enable all robots to predict the motions of their neighbors and, thus, retain the needed links to them [39]. Monitoring based on k-hop routing lets each robot search for an alternative k-path before breaking links [40].

Compared to local methods, global connectivity maintenance leads to multirobot systems with greater freedom of movement [30] but needs higher bandwidth, and thus consumes more power, for large-scale communications. Furthermore, as the size of the network increases, global connectivity maintenance increases the communication delays and, hence, severely restricts the maximum speed of the multirobot system and makes its behavior sluggish. Herein, the local connectivity preservation approach side-steps these limitations.

B. Passive Bilateral Teleoperation

Because the local robot–communications–remote robot system, also known as the teleoperator, exchanges energy with the operator and the environment, also known as the external terminators, finite gain stability and passivity [41] are fruitful concepts for analysis and design in bilateral teleoperation. In particular, a small-gain approach with projected force reflection stabilizes the teleoperation for human operators satisfying certain assumptions [42], and scattered communications guarantee $\mathcal{L}_2$-stability for users with arbitrary gains [43]. Nonetheless, the designs need the operator's admittance or damping, which generally depend on the specific tasks and actions.

Alternatively, passivity-based control assumes passive human users [44] or passivating human controllers [45] and passivates the teleoperator using energy monitoring or Lyapunov-like approaches. Energy monitoring stems from the seminal time-domain passivity approach [46], whose passivity controllers inject sufficient damping after observing active behaviors and whose position drift can be mitigated by appropriate position and velocity transmissions [47]. The passive-set-position modulation control injects fixed damping to the local and the remote robots and adapts their set positions [48]. A two-layer strategy includes nominal controllers in the top layer, to define the desired behaviors, and interconnected [49] or separated [50] energy tanks in the bottom layer, to regulate the level of passivity. From a port-Hamiltonian perspective, the energy tanks are virtual dynamical systems interconnected with the physical robots in a power-conserving way to control the passivity margin of the teleoperator [51].

Lyapunov-like approaches devise controllers by investigating the storage functions of all components of the teleoperation loop [52]. Scattered communications guarantee passive transmissions between the local and the remote robots for constant communication delays [53]. Impedance matching eliminates the wave reflections caused by scattering [54]. Interestingly, scattering-based control becomes proportional–derivative plus damping (PD+d) control for symmetric impedance matching [55]. A simpler proportional plus damping (P+d) control also guarantees teleoperator passivity [56]. For time-varying delays, P+d control outperforms the PD+d policy [57] and leads to linear matrix inequality design criteria [58]. Adaptive strategies compensate gravity and estimate uncertain parameters [59]–[61].

Herein, the design principle of Lyapunov-like approaches guides the design of the interconnections of the users' local robots to their respective leader remote robots in the RMRS

and explicitly guarantees the containment control of the RMRS in the steady state.

C. Connectivity-Preserving Swarm Teleoperation

The interplay between the couplings among the robots of the RMRS and the couplings of the users' local robots to the RMRS is the key challenge in connectivity-preserving bilateral swarm teleoperation. On the one hand, as some remote robots track the local robots, all other remote robots must self-coordinate to maintain the RMRS connected. On the other hand, feeding the forces that interconnect the remote robots back to the users may lead to detrimental motion deviations of their local robots [62] and threaten both the connectivity of the RMRS and the stability of the bilateral teleoperation.

Prior controllers rely on unbounded potentials to preserve the connectivity of the RMRS throughout the bilateral teleoperation. An unbounded potential fusing multiple constraints leads to a gradient controller that preserves the global connectivity of a teleoperated RMRS when combined with decentralized algebraic connectivity estimation [63]. An additional communication channel permits to passively tele-alter the degree of connectivity, and hence to improve the flexibility, of the RMRS [64]. Yet, it also inherits the drawbacks of decentralized algebraic connectivity estimation: stringent requirements on the communication bandwidth and sluggish robot motions. An unbounded potential sustains all interconnections among the remote robots and permits to bound the storage function of the overall system to guarantee both the connectivity of the RMRS and the closed-loop passivity of the teleoperator [65].

In contrast to the existing strategies, this article derives its control from a bounded potential that lends itself to extensions to address time-delayed communications among, and bounded actuation of, the remote robots. The proposed control avails of an appropriate decomposition of the overall dynamics and of the tree topology of the RMRS to strategically upper bound the energy stored in the RMRS. For passive teleoperation, the leader remote robots of the RMRS keep their couplings to the local robots lossless by updating their control gains based on the information that they receive from the local robots. An innovative feedforward–feedback control design renders the communications between the local and the remote robots passive in the presence of time-varying delays. Explicit containment control of the RMRS in steady-state multiuser teleoperation is the most conspicuous feature of the proposed design.

Nomenclature: Throughout this article, bold upper- and lowercase letters indicate matrices and vectors, respectively; regular fonts indicate scalars; the superscript $^{\mathsf{T}}$ denotes the transpose of a matrix or vector; $\mathbf{A} \otimes \mathbf{B}$ is the Kronecker product of the matrices $\mathbf{A}$ and $\mathbf{B}$; $\mathbf{A} \succeq \mathbf{B}$ and $\mathbf{A} \succ \mathbf{B}$ imply that $\mathbf{A} - \mathbf{B}$ is positive semidefinite and positive definite, respectively; $\mathbf{I}_n$ is the $n \times n$ identity matrix; $\mathbf{0}$ denotes a matrix or vector of appropriate dimensions with all entries 0; $\mathbf{1}_n$ and $\mathbf{0}_n$ are n-dimensional column vectors with all elements 1 and 0, respectively; $\mathrm{Diag}\{\mathbf{M}_i\}$ is a block diagonal matrix, whose ith diagonal block is $\mathbf{M}_i$; $\|\mathbf{v}\|$ is the Euclidean norm of $\mathbf{v} = (v_1, \ldots, v_n)^{\mathsf{T}}$; $\mathrm{diag}\{\mathbf{v}\}$ is a square diagonal matrix, whose ith diagonal element is v_i; $\tanh(\mathbf{v}) = (\tanh(v_1), \ldots, \tanh(v_n))^{\mathsf{T}}$ with $\tanh(\cdot)$ the hyperbolic tangent function; $\tanh^2(\mathbf{v}) = (\tanh(v_1)^2, \ldots, \tanh(v_n)^2)^{\mathsf{T}}$; the operator $\to$ indicates that the left-hand side approaches the right-hand side; the time argument of all variables is omitted when clear from the context; and the notations $|\mathbf{v}| = (|v_1|, \ldots, |v_n|)^{\mathsf{T}}$, $\mathbf{v}^2 = (v_1^2, \ldots, v_n^2)^{\mathsf{T}}$, and $\mathbf{v} \geq \mathbf{0}$ and $\mathbf{v} > \mathbf{0}$ indicating that $v_i \geq 0$ and $v_i > 0$ for all $i = 1, \ldots, n$, respectively, help save space.

III. Preliminaries

This section recalls relevant algebraic graph theory and models the bilateral multirobot teleoperator using the Euler–Lagrange (EL) formalism.

A. Graph Theory

A time-varying undirected graph $\mathcal{G}(t) = \{\mathcal{V}, \mathcal{E}(t)\}$ can encode the interactions within an RMRS. Specifically, the vertex set $\mathcal{V} = \{1, \ldots, N\}$ collects the indices of all the robots. The edge set $\mathcal{E}(t) \subset \mathcal{V} \times \mathcal{V}$ includes all bidirectional communication links (i, j) between the pairs of distinct robots i and j at time t. Let $\mathcal{N}_i(t) = \{j \in \mathcal{V} \mid (i, j) \in \mathcal{E}(t)\}$ be the set of neighbors j of robot i at time t. The degree $d_i(t)$ of robot i is then the cardinality of $\mathcal{N}_i(t)$, $d_i(t) = |\mathcal{N}_i(t)|$. The $N \times N$ diagonal degree matrix $\mathbf{D}(t)$ has $d_i(t)$ as its ith diagonal element. If robot j is a neighbor of robot i, $j \in \mathcal{N}_i(t)$, robot j is said to be adjacent to robot i. Let $a_{ij}(t) = 1$ if $j \in \mathcal{N}_i(t)$, and $a_{ij}(t) = 0$ otherwise. The $N \times N$ adjacency matrix $\mathbf{A}(t)$ has $a_{ij}(t)$ as its (i, j)th component. Then, $\overline{\mathbf{L}}(t) = \mathbf{D}(t) - \mathbf{A}(t)$ is the unweighted Laplacian matrix of the graph. Because $\mathcal{G}(t)$ is undirected, $\mathbf{A}(t)$ and $\overline{\mathbf{L}}(t)$ are symmetric.

Let there be M pairs of mutually adjacent robots in the RMRS. The cardinality of the edge set $\mathcal{E}(t)$ is then $|\mathcal{E}(t)| = M$. An oriented version of $\mathcal{G}(t)$ can be derived by assigning a unique index $k = 1, \ldots, M$ and an arbitrary orientation to every link $(i, j) \in \mathcal{E}(t)$. Furthermore, an $N \times M$ incidence matrix $\mathbf{B}(t)$ can be associated with the oriented graph that satisfies $\overline{\mathbf{L}}(t) = \mathbf{B}(t)\mathbf{B}^{\mathsf{T}}(t)$ and induces the edge Laplacian matrix $\mathbf{L}_e(t)$ for $\mathcal{G}(t)$ through $\mathbf{L}_e(t) = \mathbf{B}^{\mathsf{T}}(t)\mathbf{B}(t)$.

A path in $\mathcal{G}(t)$ is a sequence of edges that joins a sequence of distinct vertices. If a path exists between every pair of distinct vertices, then $\mathcal{G}(t)$ is connected. A tree is a connected graph with the minimum number of edges. If $\mathcal{G}(t)$ is a tree, the smallest eigenvalue of its edge Laplacian $\mathbf{L}_e(t)$ is positive, i.e., $\lambda_L > 0$. For more details on algebraic graph theory, refer to [66, Ch. 2].

B. System Dynamics

Let a bilateral teleoperator have N_l local robots and an RMRS with N_r remote robots, $N_r \geq N_l \geq 1$. The communication network of the RMRS is encoded by $\mathcal{G}(t) = \{\mathcal{V}, \mathcal{E}(t)\}$, in which $\mathcal{V} = \{1, \ldots, N_r\}$ collects the indices of all the remote robots. Furthermore, let the local robot i be connected to the remote robot i across the Internet. Then, as in [10], the first N_l remote robots are leaders and the remaining $N_r - N_l$ remote robots are followers. After local gravity compensation, the EL dynamics of the local robots are

$$\mathbf{M}_{li}(\mathbf{x}_{li})\ddot{\mathbf{x}}_{li} + \mathbf{C}_{li}(\mathbf{x}_{li}, \dot{\mathbf{x}}_{li})\dot{\mathbf{x}}_{li} = \mathbf{f}_{li} + \mathbf{f}_{hi} \tag{1}$$

for $i = 1, \ldots, N_l$, and the EL dynamics of the remote robots are

$$\mathbf{M}_{ri}(\mathbf{x}_{ri})\ddot{\mathbf{x}}_{ri} + \mathbf{C}_{ri}(\mathbf{x}_{ri}, \dot{\mathbf{x}}_{ri})\dot{\mathbf{x}}_{ri} = \mathbf{f}_{ri} \tag{2}$$

for $i = 1, \ldots, N_r$, where $\mathbf{x}_*$, $\dot{\mathbf{x}}_*$, and $\ddot{\mathbf{x}}_*$ with the subscript $* \in \{li, ri\}$ are the n-dimensional positions, velocities, and accelerations of the corresponding robots, $\mathbf{M}_*(\mathbf{x}_*)$ and $\mathbf{C}_*(\mathbf{x}_*, \dot{\mathbf{x}}_*)$ are the matrices of inertia and of Coriolis and centrifugal effects, respectively, $\mathbf{f}_*$ are the control inputs, and $\mathbf{f}_{hi}$ is the force applied by user i on their local robot $i, i = 1, \ldots, N_l$. Some properties of the above EL dynamics have been presented in [67] to facilitate the control design and the energy analysis in the following sections.

Let the communication range of all the remote robots be $r > 0$. Then, the remote robots i and j can exchange information at time $t \geq 0$ if they are within distance $\|\mathbf{x}_{rij}(t)\| < r$ of each other, where $\mathbf{x}_{rij}(t) = \mathbf{x}_{ri}(t) - \mathbf{x}_{rj}(t)$. Notably, initially, nonadjacent remote robots $(i, j) \notin \mathcal{E}(0)$ do not interact at a later time $t \geq 0$ even if $\|\mathbf{x}_{rij}(t)\| < r$. This condition streamlines the presentation, although is not required by the proposed design. The design relies on the following assumptions.

- A1 The human users are passive, i.e., $\int_0^t \dot{\mathbf{x}}_{li}^{\mathsf{T}}(\tau)\mathbf{f}_{hi}(\tau)d\tau < +\infty$ for all $i = 1, \ldots, N_l$ and $t \geq 0$.
- A2 The users apply forces that are bounded by $|\mathbf{f}_{hi}(t)| \leq \overline{\mathbf{f}}_{hi}$ componentwisely and have finite time derivatives $\left\|\dot{\mathbf{f}}_{hi}(t)\right\| < +\infty, \forall i = 1, \ldots, N_l$.
- A3 The RMRS starts from rest, $\dot{\mathbf{x}}_{ri}(0) = \mathbf{0}, \forall i = 1, \ldots, N_r$.
- A4 The initial communication network $\mathcal{G}(0)$ of the RMRS is a tree, and $\|\mathbf{x}_{rij}(0)\| < r - \epsilon$ with $\epsilon > 0, \forall (i, j) \in \mathcal{E}(0)$.
- A5 The time-varying communication delays $T_*(t)$ between the local robots and the RMRS are bounded and have finite time derivatives, i.e., $0 \leq T_*(t) \leq \overline{T}_* < +\infty$ and $\left|\dot{T}_*(t)\right| < +\infty$ for $* = li, ri, \forall i = 1, \ldots, N_l$ and $\forall t \geq 0$.

Here, Assumption A1 implies that the human users can inject a finite amount of energy into the teleoperator. Assumption A2 limits the user-induced perturbations on the connectivity of the RMRS. Assumptions A3 and A4 together offer a robustness margin for connectivity maintenance. Finally, Assumption A5 upper bounds the delays with which the connected local and leader remote robots receive the state of each other.

Because the proposed design preserves all the initial communication links, the communication network of the RMRS is invariant, i.e., $\mathcal{G}(t) = \mathcal{G}(0)$, $\forall t \geq 0$. Hence, the remainder of this article indicates the degree, adjacency, incidence, and edge Laplacian matrices of the communication network $\mathcal{G}(t)$ of the RMRS by $\mathbf{D}$, $\mathbf{A}$, $\mathbf{B}$, and $\mathbf{L}_e$, respectively, without time arguments.

IV. Main Results

An innovative decomposition of the overall dynamics permits to integrate the analyses of the connectivity of the RMRS and of the closed-loop passivity of the teleoperator into a unified paradigm. This section introduces the new decomposition in steps, starting with a control design for delay-free teleoperation. It then augments the design to incorporate time-delayed communications between the local robots and the RMRS. The analyses of the steady-state teleoperation and of containment control end the section.

A. Teleoperation With No Delay

This section develops a passivity-based control that ensures the connectivity of the RMRS and the passivity of the teleoperator in this order of priority. Two lemmas summarize the conditions for selecting and updating the various control gains.

1) Controller Design: Define a sliding variable $\mathbf{s}_i$ for every remote robot $i = 1, \ldots, N_r$ by

$$\mathbf{s}_i = \begin{cases} \dot{\mathbf{x}}_{ri} + \sigma\boldsymbol{\theta}_{ri} + \eta\boldsymbol{\theta}_{lri}, & i = 1, \ldots, N_l \\ \dot{\mathbf{x}}_{ri} + \sigma\boldsymbol{\theta}_{ri}, & i = N_l + 1, \ldots, N_r \end{cases} \tag{3}$$

where σ and η are positive constants, $\boldsymbol{\theta}_{lri}$ connects the leader remote robot i to its associated local robot i by

$$\boldsymbol{\theta}_{lri} = \overline{\mathbf{F}}_{hi} \cdot \tanh\left[K_{lri}(\mathbf{x}_{ri} - \mathbf{x}_{li})\right]$$

with $\overline{\mathbf{F}}_{hi} = \text{diag}\{\overline{\mathbf{f}}_{hi}\}$ and $K_{lri} > 0$, and $\boldsymbol{\theta}_{ri}$ couples the remote robot i to its neighbors $j \in \mathcal{N}_i$ by

$$\boldsymbol{\theta}_{ri} = \sum_{j \in \mathcal{N}_i} \nabla_i \psi(\|\mathbf{x}_{rij}\|)$$

with $\nabla_i \psi(\|\mathbf{x}_{rij}\|)$ the partial derivative of a bounded potential function $\psi(\|\mathbf{x}_{rij}\|)$ with respect to $\mathbf{x}_{ri}$, where

$$\psi(\|\mathbf{x}_{rij}\|) = \frac{P\|\mathbf{x}_{rij}\|^2}{r^2 - \|\mathbf{x}_{rij}\|^2 + Q}$$

with $P > 0$ and $Q > 0$, and

$$\nabla_i \psi(\|\mathbf{x}_{rij}\|) = \frac{2P(r^2 + Q)}{\left(r^2 - \|\mathbf{x}_{rij}\|^2 + Q\right)^2}(\mathbf{x}_{ri} - \mathbf{x}_{rj}).$$

Note that $\psi(\|\mathbf{x}_{rij}\|)$ is strictly increasing and bounded by $0 \leq \psi(\|\mathbf{x}_{rij}\|) < \psi_{\max} = Pr^2/Q$ for $\|\mathbf{x}_{rij}\| < r$.

Let $\mathbf{L}(\mathbf{x}_r) = [l_{ij}(\mathbf{x}_r)]$ be the $N_r \times N_r$ weighted Laplacian matrix of the tree communication network of the RMRS. The (i, j)th element $l_{ij}(\mathbf{x}_r)$ of $\mathbf{L}(\mathbf{x}_r)$ is given by

$$l_{ij}(\mathbf{x}_r) = \begin{cases} -\frac{2P(r^2+Q)}{(r^2 - \|\mathbf{x}_{rij}\|^2 + Q)^2}, & j \neq i \text{ and } j \in \mathcal{N}_i \\ 0, & j \neq i \text{ and } j \notin \mathcal{N}_i \\ -\sum_{k \neq i} l_{ik}(\mathbf{x}_r), & j = i. \end{cases}$$

The notation $\mathbf{L}(\mathbf{x}_r)$ indicates the dependence of the weighted Laplacian matrix on the positions $\mathbf{x}_r = (\mathbf{x}_{r1}^{\mathsf{T}}, \ldots, \mathbf{x}_{rN_r}^{\mathsf{T}})^{\mathsf{T}}$ of the remote robots. This dependence arises because $l_{ij}(\mathbf{x}_r) = l_{ji}(\mathbf{x}_r)$ depends on the distance $\|\mathbf{x}_{rij}\|$ between the pair of adjacent remote robots $(i, j) \in \mathcal{E}$. Let $\mathbf{l}_i(\mathbf{x}_r)$ be the ith column of $\mathbf{L}(\mathbf{x}_r)$. Then, $\boldsymbol{\theta}_{ri}$ becomes

$$\boldsymbol{\theta}_{ri} = \left[\mathbf{l}_i^{\mathsf{T}}(\mathbf{x}_r) \otimes \mathbf{I}_n\right]\mathbf{x}_r, \quad i = 1, \ldots, N_r.$$

The sliding variables $\mathbf{s}_i$ in (3) for the RMRS can then be reorganized into

$$\Pi_1: \quad \dot{\mathbf{x}}_r = -\sigma\left[\mathbf{L}(\mathbf{x}_r) \otimes \mathbf{I}_n\right]\mathbf{x}_r + \mathbf{s} - \eta\mathbf{u}_{lr} \tag{4}$$

where $\mathbf{L}^{\mathsf{T}}(\mathbf{x}_r) = \mathbf{L}(\mathbf{x}_r)$, and $\mathbf{s} - \eta\mathbf{u}_{lr}$ is the input to the dynamical system Π_1, with $\mathbf{s} = (\mathbf{s}_1^{\mathsf{T}}, \ldots, \mathbf{s}_{N_r}^{\mathsf{T}})^{\mathsf{T}}$ and $\mathbf{u}_{lr} =$

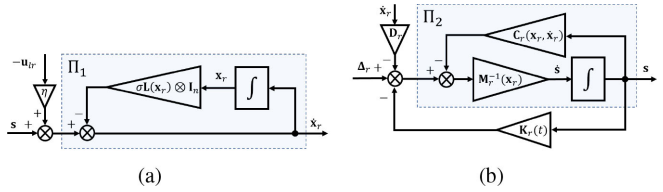

Fig. 1. Input–output diagrams of the systems Π_1 in (4) and Π_2 in (8). (a) Input–output diagram of Π_1. (b) Input–output diagram of Π_2.

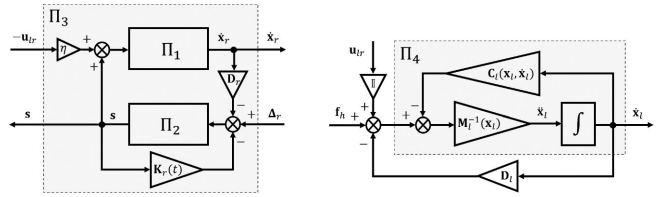

Fig. 2. Input–output diagrams (a) of the RMRS Π_3 (the feedback interconnection of Π_1 and Π_2) and (b) of the local robots Π_4.

$(\boldsymbol{\theta}_{lr1}^{\mathsf{T}}, \ldots, \boldsymbol{\theta}_{lrN_l}^{\mathsf{T}}, \mathbf{0}^{\mathsf{T}}, \ldots, \mathbf{0}^{\mathsf{T}})^{\mathsf{T}}$ [see Fig. 1(a)]. The sliding variables also convert the dynamics (2) of the RMRS into

$$\mathbf{M}_{ri}(\mathbf{x}_{ri})\dot{\mathbf{s}}_i + \mathbf{C}_{ri}(\mathbf{x}_{ri}, \dot{\mathbf{x}}_{ri})\mathbf{s}_i = \sigma\boldsymbol{\Delta}_{rri} + \eta\boldsymbol{\Delta}_{lri} + \mathbf{f}_{ri} \quad (5)$$

where the mismatched dynamics are $\boldsymbol{\Delta}_{rri} = \mathbf{M}_{ri}(\mathbf{x}_{ri})\dot{\boldsymbol{\theta}}_{ri} + \mathbf{C}_{ri}(\mathbf{x}_{ri}, \dot{\mathbf{x}}_{ri})\boldsymbol{\theta}_{ri}$, $\boldsymbol{\Delta}_{lri} = \mathbf{M}_{ri}(\mathbf{x}_{ri})\dot{\boldsymbol{\theta}}_{lri} + \mathbf{C}_{ri}(\mathbf{x}_{ri}, \dot{\mathbf{x}}_{ri})\boldsymbol{\theta}_{lri}$ if $i = 1, \ldots, N_l$, and $\boldsymbol{\Delta}_{lri} = \mathbf{0}$ otherwise. Note that $\boldsymbol{\Delta}_{rri}$ are caused by the couplings among the remote robots, whereas $\boldsymbol{\Delta}_{lri}$ are caused by the couplings between the local robots and the leader remote robots.

Let the controllers of the remote robots be

$$\mathbf{f}_{ri} = -K_{ri}(t)\mathbf{s}_i - D_{ri}\dot{\mathbf{x}}_{ri} \quad (6)$$

where $D_{ri} > 0$ and $K_{ri}(t)$ are to be determined. After stacking the mismatched dynamics of the remote robots into

$$\boldsymbol{\Delta}_r = \left(\sigma\boldsymbol{\Delta}_{rr1}^{\mathsf{T}} + \eta\boldsymbol{\Delta}_{lr1}^{\mathsf{T}}, \ldots, \sigma\boldsymbol{\Delta}_{rrN_r}^{\mathsf{T}} + \eta\boldsymbol{\Delta}_{lrN_r}^{\mathsf{T}}\right)^{\mathsf{T}} \quad (7)$$

and combining their inertia and Christoffel matrices, respectively, into $\mathbf{M}_r(\mathbf{x}_r) = \mathrm{Diag}\{\mathbf{M}_{ri}(\mathbf{x}_{ri})\}$ and $\mathbf{C}_r(\mathbf{x}_r, \dot{\mathbf{x}}_r) = \mathrm{Diag}\{\mathbf{C}_{ri}(\mathbf{x}_{ri}, \dot{\mathbf{x}}_{ri})\}$, the dynamics (5) of the RMRS under the control (6) become

$$\Pi_2: \quad \mathbf{M}_r(\mathbf{x}_r)\dot{\mathbf{s}} + \mathbf{C}_r(\mathbf{x}_r, \dot{\mathbf{x}}_r)\mathbf{s} = \boldsymbol{\Delta}_r - \mathbf{K}_r(t)\mathbf{s} - \mathbf{D}_r\dot{\mathbf{x}}_r \quad (8)$$

with $\mathbf{K}_r(t) = \mathrm{Diag}\{K_{ri}(t)\mathbf{I}_n\}$ and $\mathbf{D}_r = \mathrm{Diag}\{D_{ri}\mathbf{I}_n\}$. The system Π_2 has the state $\mathbf{s}$, the dynamic feedback $-\mathbf{K}_r(t)\mathbf{s}$, and the input $-\mathbf{D}_r\dot{\mathbf{x}}_r$ and is perturbed by $\boldsymbol{\Delta}_r$ [see Fig. 1(b)].

Thus, the sliding variables $\mathbf{s}_i$ designed in (3) restructure the RMRS (2) under the control of (6) into the negative feedback interconnection Π_3 of the dynamical systems Π_1 in (4) and Π_2 in (8): the output $\mathbf{s}$ of Π_2 is the input to Π_1, and the output $\dot{\mathbf{x}}_r$ of Π_1 is negatively fed back to Π_2. As shown in Fig. 2(a), the feedback interconnected system Π_3 has two inputs: 1) $-\mathbf{u}_{lr}$, from the couplings between the local robots and the RMRS; and 2) $\boldsymbol{\Delta}_r$, the uncertainty in the reshaped dynamics of the RMRS.

The force feedback to the users is obtained by connecting their local robots to the associated leader remote robots via

$$\mathbf{f}_{li} = \boldsymbol{\theta}_{lri} - D_{li}\dot{\mathbf{x}}_{li}, \quad i = 1, \ldots, N_l \quad (9)$$

with $D_{li} > 0$. After letting $\mathbf{M}_l(\mathbf{x}_l) = \mathrm{Diag}\{\mathbf{M}_{li}(\mathbf{x}_{li})\}$ and $\mathbf{C}_l(\mathbf{x}_l, \dot{\mathbf{x}}_l) = \mathrm{Diag}\{\mathbf{C}_{li}(\mathbf{x}_{li}, \dot{\mathbf{x}}_{li})\}$, all the local robots (1) under the control of (9) form

$$\Pi_4: \quad \mathbf{M}_l(\mathbf{x}_l)\ddot{\mathbf{x}}_l + \mathbf{C}_l(\mathbf{x}_l, \dot{\mathbf{x}}_l)\dot{\mathbf{x}}_l = \mathbf{f}_h + \mathbb{I}\mathbf{u}_{lr} - \mathbf{D}_l\dot{\mathbf{x}}_l \quad (10)$$

where $\mathbf{x}_l = (\mathbf{x}_{l1}^{\mathsf{T}}, \ldots, \mathbf{x}_{lN_l}^{\mathsf{T}})^{\mathsf{T}}$ and $\mathbf{f}_h = (\mathbf{f}_{h1}^{\mathsf{T}}, \ldots, \mathbf{f}_{hN_l}^{\mathsf{T}})^{\mathsf{T}}$ group the positions and the user forces of all the local robots, and $\mathbb{I} = [\mathbf{I}_{N_l}\ \mathbf{0}_{N_l \times (N_r - N_l)}] \otimes \mathbf{I}_n$ and $\mathbf{D}_l = \mathrm{Diag}\{D_{li}\mathbf{I}_n\}$. As seen in Fig. 2(b), Π_4 has two inputs, $\mathbf{f}_h$ from all the users and $\mathbf{u}_{lr}$ from all the couplings between the local robots and the RMRS, and one output, $\dot{\mathbf{x}}_l$.

2) Connectivity Maintenance: This section shows that, with no prerequisite for closed-loop passivity, the connectivity of the RMRS can be preserved by selecting appropriate gains for the designed system Π_3. Maintaining the tree communication network $\mathcal{G}(t)$ of the RMRS is equivalent to rendering the edge set $\mathcal{E}(t)$ invariant. Therefore, the proof shows how to choose gains to shape the energy production of Π_3 to guarantee that all the remote robots that are initially adjacent remain adjacent throughout time, that is, $\|\mathbf{x}_{rij}(t)\| < r, \forall (i,j) \in \mathcal{E}(0)$ and $\forall t \geq 0$.

Because Π_3 is the negative feedback interconnection of Π_1 and Π_2 [see Fig. 2(a)], its energy production depends on the energy productions of Π_1 and Π_2. Define the storage function of Π_1 by

$$V_1 = \frac{\sigma}{2}\sum_{i=1}^{N_r}\sum_{j\in\mathcal{N}_i}\psi(\|\mathbf{x}_{rij}\|). \quad (11)$$

After stacking all $\boldsymbol{\theta}_{ri}$, $i = 1, \ldots, N_r$, into $\boldsymbol{\theta}_r$ by

$$\boldsymbol{\theta}_r = \left(\boldsymbol{\theta}_{r1}^{\mathsf{T}}, \ldots, \boldsymbol{\theta}_{rN_r}^{\mathsf{T}}\right)^{\mathsf{T}} = [\mathbf{L}(\mathbf{x}_r) \otimes \mathbf{I}_n]\,\mathbf{x}_r$$

the time derivative of V_1 along the dynamics (4) of Π_1 is

$$\begin{aligned}\dot{V}_1 &= \sigma\sum_{i=1}^{N_r}\sum_{j\in\mathcal{N}_i}\dot{\mathbf{x}}_{ri}^{\mathsf{T}}\nabla_i\psi(\|\mathbf{x}_{rij}\|) = \sigma\sum_{i=1}^{N_r}\dot{\mathbf{x}}_{ri}^{\mathsf{T}}\boldsymbol{\theta}_{ri} = \sigma\dot{\mathbf{x}}_r^{\mathsf{T}}\boldsymbol{\theta}_r \\ &= \sigma\dot{\mathbf{x}}_r^{\mathsf{T}}[\mathbf{L}(\mathbf{x}_r) \otimes \mathbf{I}_n]\,\mathbf{x}_r = \dot{\mathbf{x}}_r^{\mathsf{T}}\mathbf{s} - \eta\dot{\mathbf{x}}_r^{\mathsf{T}}\mathbf{u}_{lr} - \dot{\mathbf{x}}_r^{\mathsf{T}}\dot{\mathbf{x}}_r \quad (12)\end{aligned}$$

which implies that the subsystem Π_1 is output strictly passive with the input $\mathbf{s} - \eta\mathbf{u}_{lr}$ and the output $\dot{\mathbf{x}}_r$.

Furthermore, let the storage function of Π_2 be the following anisotropic scaling of its kinetic energy:

$$V_2 = \frac{1}{2}\sum_{i=1}^{N_r}\frac{1}{D_{ri}}\mathbf{s}_i^{\mathsf{T}}\mathbf{M}_{ri}(\mathbf{x}_{ri})\mathbf{s}_i. \quad (13)$$

After using the skew-symmetry of $\dot{\mathbf{M}}_{ri}(\mathbf{x}_{ri}) - 2\mathbf{C}_{ri}(\mathbf{x}_{ri}, \dot{\mathbf{x}}_{ri})$, the time derivative of V_2 along the dynamics (8) of Π_2 is

$$\dot{V}_2 = \frac{1}{2}\sum_{i=1}^{N_r}\frac{1}{D_{ri}}\mathbf{s}_i^{\mathsf{T}}\left[\dot{\mathbf{M}}_{ri}(\mathbf{x}_{ri}) - 2\mathbf{C}_{ri}(\mathbf{x}_{ri}, \dot{\mathbf{x}}_{ri})\right]\mathbf{s}_i$$

$$+\sum_{i=1}^{N_r}\frac{1}{D_{ri}}\mathbf{s}_i^{\mathsf{T}}\left[\sigma\boldsymbol{\Delta}_{rri}+\eta\boldsymbol{\Delta}_{lri}-K_{ri}(t)\mathbf{s}_i-D_{ri}\dot{\mathbf{x}}_{ri}\right]$$
$$=\mathbf{s}^{\mathsf{T}}\mathbf{D}_r^{-1}\boldsymbol{\Delta}_r-\mathbf{s}^{\mathsf{T}}\dot{\mathbf{x}}_r-\mathbf{s}^{\mathsf{T}}\mathbf{D}_r^{-1}\mathbf{K}_r(t)\mathbf{s} \tag{14}$$

which implies that the subsystem Π_2 is output strictly passive with the input $\boldsymbol{\Delta}_r-\mathbf{D}_r\dot{\mathbf{x}}_r$ and the output $\mathbf{s}$.

Then, the storage function of the system Π_3 is

$$V_3=V_1+V_2 \tag{15}$$

which, by (12) and (14), varies according to

$$\dot{V}_3=\mathbf{s}^{\mathsf{T}}\mathbf{D}_r^{-1}\boldsymbol{\Delta}_r-\eta\dot{\mathbf{x}}_r^{\mathsf{T}}\mathbf{u}_{lr}-\dot{\mathbf{x}}_r^{\mathsf{T}}\dot{\mathbf{x}}_r-\mathbf{s}^{\mathsf{T}}\mathbf{D}_r^{-1}\mathbf{K}_r(t)\mathbf{s} \tag{16}$$

where the zero sum of $\dot{\mathbf{x}}_r^{\mathsf{T}}\mathbf{s}$ in $\dot{V}_1$ and $-\mathbf{s}^{\mathsf{T}}\dot{\mathbf{x}}_r$ in $\dot{V}_2$ proves that the negative feedback interconnection of Π_1 and Π_2 [see Fig. 2(a)] is power-preserving. Equation (16) implies that Π_3 is output strictly passive with the input $(-\mathbf{u}_{lr}^{\mathsf{T}},\boldsymbol{\Delta}_r^{\mathsf{T}})^{\mathsf{T}}$ and the output $(\dot{\mathbf{x}}_r^{\mathsf{T}},\mathbf{s}^{\mathsf{T}})^{\mathsf{T}}$. For connectivity maintenance, V_3 should also be upper-bounded by $\sigma\psi_{\max}$ (by [68, Proposition 2]). As shown in the following, V_3 can be limited appropriately by controlling the excess of output passivity of Π_3.

Let $\widetilde{\mathbf{x}}_r=[\mathbf{B}^{\mathsf{T}}\otimes\mathbf{I}_n]\mathbf{x}_r$ and define a diagonal matrix $\mathbf{W}(\mathbf{x}_r)$, whose diagonal collects the weights $l_{ij}(\mathbf{x}_r)$ of the N_r-1 edges $(i,j)\in\mathcal{E}$ of the tree network of the RMRS. Then, the edge Laplacian $\mathbf{L}_e$ serves to bound V_1 by

$$\begin{aligned}V_1&=\sum_{(i,j)\in\mathcal{E}}\frac{\sigma\left(r^2-\|\mathbf{x}_{rij}\|^2+Q\right)^3}{4P(r^2+Q)^2}\left\|\nabla_i\psi(\|\mathbf{x}_{rij}\|)\right\|^2\\&\le\frac{\sigma(r^2+Q)}{4P}\widetilde{\mathbf{x}}_r^{\mathsf{T}}\left[\mathbf{W}(\mathbf{x}_r)\otimes\mathbf{I}_n\right]^{\mathsf{T}}\left[\mathbf{W}(\mathbf{x}_r)\otimes\mathbf{I}_n\right]\widetilde{\mathbf{x}}_r\\&\le\frac{\sigma(r^2+Q)}{4\lambda_L P}\widetilde{\mathbf{x}}_r^{\mathsf{T}}\left[\mathbf{W}^{\mathsf{T}}(\mathbf{x}_r)\mathbf{L}_e\mathbf{W}(\mathbf{x}_r)\otimes\mathbf{I}_n\right]\widetilde{\mathbf{x}}_r\\&=\frac{\sigma k_r}{4\lambda_L}\mathbf{x}_r^{\mathsf{T}}\left[\mathbf{B}\mathbf{W}^{\mathsf{T}}(\mathbf{x}_r)\mathbf{B}^{\mathsf{T}}\mathbf{B}\mathbf{W}(\mathbf{x}_r)\mathbf{B}^{\mathsf{T}}\otimes\mathbf{I}_n\right]\mathbf{x}_r\\&=\frac{\sigma k_r}{4\lambda_L}\mathbf{x}_r^{\mathsf{T}}\left[\mathbf{L}^{\mathsf{T}}(\mathbf{x}_r)\mathbf{L}(\mathbf{x}_r)\otimes\mathbf{I}_n\right]\mathbf{x}_r\end{aligned} \tag{17}$$

where $k_r=(r^2+Q)/P$ and the third line results from applying $\mathbf{L}_e\succeq\lambda_L\mathbf{I}_{N_r}$ of the tree communication network of the RMRS (see [67] for detailed derivations). The dynamics in (4) and further algebraic manipulations yield

$$\frac{\sigma^2}{2}\mathbf{x}_r^{\mathsf{T}}\left[\mathbf{L}^{\mathsf{T}}(\mathbf{x}_r)\mathbf{L}(\mathbf{x}_r)\otimes\mathbf{I}_n\right]\mathbf{x}_r\le 2\dot{\mathbf{x}}_r^{\mathsf{T}}\dot{\mathbf{x}}_r+2\mathbf{s}^{\mathsf{T}}\mathbf{s}+\eta^2\mathbf{u}_{lr}^{\mathsf{T}}\mathbf{u}_{lr}$$

and V_3 can be linked to the output passivity indices of Π_3 by

$$V_3\le\frac{k_r}{2\sigma\lambda_L}\left(2\dot{\mathbf{x}}_r^{\mathsf{T}}\dot{\mathbf{x}}_r+2\mathbf{s}^{\mathsf{T}}\mathbf{s}+\eta^2\mathbf{u}_{lr}^{\mathsf{T}}\mathbf{u}_{lr}\right)+\frac{1}{2}\mathbf{s}^{\mathsf{T}}\mathbf{D}_r^{-1}\boldsymbol{\Lambda}_r\mathbf{s} \tag{18}$$

where $\boldsymbol{\Lambda}_r=\mathrm{Diag}\{\lambda_{ri}\mathbf{I}_n\}$ with $\lambda_{ri}\mathbf{I}_n\succeq\mathbf{M}_{ri}(\mathbf{x}_{ri})$ for every remote robot $i=1,\ldots,N_r$.

Similarly, the power supplied to the system Π_3 through the port $(-\mathbf{u}_{lr},\dot{\mathbf{x}}_r)$ can be measured by

$$-\eta\dot{\mathbf{x}}_r^{\mathsf{T}}\mathbf{u}_{lr}\le\dot{\mathbf{x}}_r^{\mathsf{T}}\dot{\mathbf{x}}_r/4+\eta^2\mathbf{u}_{lr}^{\mathsf{T}}\mathbf{u}_{lr}. \tag{19}$$

The power injected into Π_3 by the mismatched dynamics $\boldsymbol{\Delta}_r$, resulting from the state transformation (5), is upper-bounded in [67, Appendix A] by

$$\mathbf{s}^{\mathsf{T}}\mathbf{D}_r^{-1}\boldsymbol{\Delta}_r\le\mathbf{1}_{N_rn}^{\mathsf{T}}\mathbf{D}_r^{-1}\left[\eta\mathbb{I}^{\mathsf{T}}\mathbb{I}+\sigma\left(3\mathbf{D}+2\mathbf{A}\right)\otimes\mathbf{I}_n\right]\dot{\mathbf{x}}_r^2+\mathbf{s}^{\mathsf{T}}\mathbf{D}_r^{-1}\boldsymbol{\Gamma}_1^c(t)\mathbf{s}+\eta^2\overline{\mathbf{f}}_h^{\mathsf{T}}\mathbb{I}\mathbf{D}_r^{-1}\mathbb{I}^{\mathsf{T}}\overline{\mathbf{f}}_h \tag{20}$$

where $\boldsymbol{\Gamma}_1^c(t)=\eta\mathbb{I}^{\mathsf{T}}\boldsymbol{\Gamma}_{lr}^c(t)\mathbb{I}+\sigma\boldsymbol{\Gamma}_{rr}(t)$, with $\boldsymbol{\Gamma}_{lr}^c(t)$ a function of the position and the velocity differences between the leader remote robots and their associated local robots, $\boldsymbol{\Gamma}_{rr}(t)$ a function of the displacements between the remote robots, and $\overline{\mathbf{f}}_h=(\overline{\mathbf{f}}_{h1}^{\mathsf{T}},\ldots,\overline{\mathbf{f}}_{hN_l}^{\mathsf{T}})^{\mathsf{T}}$ collects the upper bounds of all the user forces given in Assumption A2. Note that the main diagonal blocks of both $\boldsymbol{\Gamma}_{lr}^c(t)$ and $\boldsymbol{\Gamma}_{rr}(t)$ require solely one-hop exchanges of the states of the remote robots.

Together, (16)–(20) bound the power production of Π_3 by

$$\dot{V}_3\le\frac{\eta^2}{8}\overline{\mathbf{f}}_h^{\mathsf{T}}\mathbb{I}\left(9\mathbf{I}_{N_rn}+8\mathbf{D}_r^{-1}\right)\mathbb{I}^{\mathsf{T}}\overline{\mathbf{f}}_h-\frac{\sigma\lambda_L}{4k_r}V_3-\frac{1}{2}\mathbf{1}_{N_rn}^{\mathsf{T}}\mathbf{D}_r^{-1}\mathbf{D}_{cr}\dot{\mathbf{x}}_r^2-\mathbf{s}^{\mathsf{T}}\mathbf{D}_r^{-1}\mathbf{K}_{cr}(t)\mathbf{s} \tag{21}$$

after using $\mathbf{u}_{lr}^{\mathsf{T}}\mathbf{u}_{lr}\le\overline{\mathbf{f}}_h^{\mathsf{T}}\mathbb{I}\mathbb{I}^{\mathsf{T}}\overline{\mathbf{f}}_h$ and

$$\mathbf{D}_{cr}=\mathbf{D}_r-2\eta\mathbb{I}^{\mathsf{T}}\mathbb{I}-2\sigma\left(3\mathbf{D}+2\mathbf{A}\right)\otimes\mathbf{I}_n$$
$$\mathbf{K}_{cr}(t)=\mathbf{K}_r(t)-\left(\sigma\lambda_L\boldsymbol{\Lambda}_r+2k_r\mathbf{D}_r\right)/(8k_r)-\boldsymbol{\Gamma}_1^c(t).$$

The bound on $\dot{V}_3$ in (21) indicates that the maximum rate of energy injection into Π_3 is determined by $\overline{\mathbf{f}}_h$, while the excess/shortage of output passivity of Π_3 depends on V_3, $\dot{\mathbf{x}}_r$, and $\mathbf{s}$. The following lemma defines the level of passivity of Π_3 that guarantees the connectivity of the RMRS.

Lemma 1: For the RMRS (2) under the control of (6), let D_{ri} be selected and $K_{ri}(t)$ be updated to guarantee that $\mathbf{D}_r^{-1}\mathbf{D}_{cr}\mathbf{1}_{N_rn}\ge\mathbf{0}$ and $\mathbf{K}_{cr}(t)\succeq\mathbf{0}$ and such that

$$V_3(0)+\frac{k_r\eta^2}{2\sigma\lambda_L}\overline{\mathbf{f}}_h^{\mathsf{T}}\mathbb{I}\left(9\mathbf{I}_{N_rn}+8\mathbf{D}_r^{-1}\right)\mathbb{I}^{\mathsf{T}}\overline{\mathbf{f}}_h<\sigma\psi_{\max}. \tag{22}$$

Then, the tree communication network of the RMRS remains invariant, i.e., $\mathcal{E}(t)=\mathcal{E}(0),\forall t\ge 0$.

Proof: For $\mathbf{D}_r^{-1}\mathbf{D}_{cr}\mathbf{1}_{N_rn}\ge\mathbf{0}$ and $\mathbf{K}_{cr}(t)\succeq\mathbf{0}$, Grönwall's inequality applied to (21) yields

$$V_1(t)\le V_3(t)\le\frac{k_r\eta^2}{2\sigma\lambda_L}\overline{\mathbf{f}}_h^{\mathsf{T}}\mathbb{I}\left(9\mathbf{I}_{N_rn}+8\mathbf{D}_r^{-1}\right)\mathbb{I}^{\mathsf{T}}\overline{\mathbf{f}}_h+V_3(0)\cdot\exp\left[-\sigma\lambda_L t/(4k_r)\right]<\sigma\psi_{\max}$$

and the tree communication network of the RMRS is positively invariant by [68, Proposition 2]. ■

The above proof of connectivity maintenance is by induction on time. Together with $V_2\ge 0$, [68, Proposition 2] gives a sufficient condition for preserving the tree network: $V_3(t)<\sigma\psi_{\max}$ for every $t\ge 0$. Given that $V_3(0)<\sigma\psi_{\max}$ by (22), it suffices to prove that $V_3(t)<\sigma\psi_{\max}$ if $V_3(\tau)<\sigma\psi_{\max}$ for all $\tau\in[0,t)$. The assumption that $V_3(\tau)<\sigma\psi_{\max}$ for all $\tau\in[0,t)$, namely, that the edge set $\mathcal{E}$ is invariant during the time interval $[0,t)$, precludes two logical paradoxes in the proof of $V_3(t)<\sigma\psi_{\max}$: 1) the controller (6) of every remote robot i can employ the information of all its initial neighbors $j\in\mathcal{N}_i$ in the tree network;

and 2) $\|\mathbf{x}_{rij}\| < r$ for every pair of initially adjacent remote robots $(i,j) \in \mathcal{E}(0)$.

The conditions of Lemma 1 are feasible by the Assumptions A3 and A4 in Section III-B. To illustrate this, analogous to (17), lower bound V_1 by

$$V_1 \geq \frac{\sigma \overline{k}_r Q}{4\overline{\lambda}_L P} \mathbf{x}_r^{\mathsf{T}} \left[\mathbf{L}^{\mathsf{T}}(\mathbf{x}_r) \mathbf{L}(\mathbf{x}_r) \otimes \mathbf{I}_n \right] \mathbf{x}_r \tag{23}$$

where $\overline{k}_r = Q^2/(r^2+Q)^2$ and $\overline{\lambda}_L$ is the maximum eigenvalue of $\mathbf{L}_e$. The dynamics (4) of Π_1 and the energy (13) of Π_2 together limit $V_3(0)$ by

$$V_3(0) \leq \left(1 + \frac{4\sigma \lambda_r \overline{\lambda}_L P}{\overline{k}_r D_r Q}\right) V_1(0) + \frac{\lambda_r \eta^2}{D_r} \overline{\mathbf{f}}_h^{\mathsf{T}} \overline{\mathbf{f}}_h$$

where $\lambda_r \mathbf{I}_{N_r n} \succeq \mathbf{\Lambda}_r$ and $\mathbf{D}_r \succeq D_r \mathbf{I}_{N_r n}$. Then, the condition (22) can be guaranteed by

$$V_1(0) + \alpha \overline{\mathbf{f}}_h^{\mathsf{T}} \overline{\mathbf{f}}_h < \widehat{\sigma} \psi_{\max} \tag{24}$$

where α is upper-bounded by

$$\alpha \leq \frac{\eta^2}{\sigma} \left[\frac{\overline{k}_r Q}{4\overline{\lambda}_L P} + \frac{k_r (9D_r + 8)}{2\lambda_L D_r} \right] = \overline{\alpha}$$

and $\widehat{\sigma}$ approaches σ as D_r increases. Therefore, after choosing σ and η and letting $\Delta = \overline{\alpha} \overline{\mathbf{f}}_h^{\mathsf{T}} \overline{\mathbf{f}}_h$, [68, Proposition 1] shows how to select P and Q such that $V_1(0) + \Delta < \sigma \psi_{\max}$. Then, there exist damping gains $\mathbf{D}_r$ with D_r sufficiently large to ensure (24), and thus (22), and $\mathbf{D}_{cr} \succeq \mathbf{0}$ [see [67] for the detailed derivation of (24) from (23)].

The design of the system Π_3 is motivated by the equivalence between maintaining the tree network connectivity of the remote robots and rendering the associated edge set $\mathcal{E}(t)$ invariant. The bounded potentials $\psi(\|\mathbf{x}_{rij}\|)$, of all the couplings between pairs of initially adjacent remote robots $(i,j) \in \mathcal{E}(0)$, convert the problem of rendering $\mathcal{E}(t)$ invariant into the problem of upper bounding the energy V_3 by $\sigma \psi_{\max}$. Then, the condition (22) implies that the connectivity of the RMRS (indexed by V_3) depends both on the initial energy $V_3(0)$ of Π_3 and on the energy injected into Π_3 by the connections $-\mathbf{u}_{lr}$ (with bounds $\overline{\mathbf{f}}_h$) of the RMRS to the local robots. By (15), the dependence on $V_3(0)$ of (22) constrains the initial velocities $\dot{\mathbf{x}}_{ri}(0)$ of, and the initial distances $\|\mathbf{x}_{rij}(0)\|$ between, the remote robots. The impact of the couplings between the local and the remote robots can be tuned by η^2/σ in (24). In light of (4), increasing σ strengthens the couplings between the remote robots, and reducing η attenuates the perturbing effect of $-\mathbf{u}_{lr}$. Together, the ratio η^2/σ regulates $\overline{\alpha}$ and, with it, the energy injected into Π_3 by the couplings of the RMRS to the local robots as per (24).

The uncertainty $\mathbf{\Delta}_r$ in the transformed dynamics (8) of the RMRS, which varies with the states of the remote robots, is an input to the system Π_3, whose power injection is upper-bounded by (20). Because $\mathbf{\Gamma}_{lr}^c(t)$ and $\mathbf{\Gamma}_{rr}(t)$ are time-varying, the condition $\mathbf{K}_{cr}(t) \succeq \mathbf{0}$ requests that $\mathbf{K}_r(t)$ be updated dynamically. Nevertheless, the updating of $\mathbf{K}_r(t)$ is distributed in the sense of implementation because the controls of all the remote robots rely exclusively on one-hop communications. By the definitions of $\mathbf{\Gamma}_{rr}(t)$ and $\mathbf{\Gamma}_{lr}^c(t)$ in [67, Appendix A], each follower remote robot i needs only the positions of its neighbors $j \in \mathcal{N}_i$ in the tree network, and each leader remote robot needs the positions of its neighboring remote robots and the position and velocity of its associated local robot.

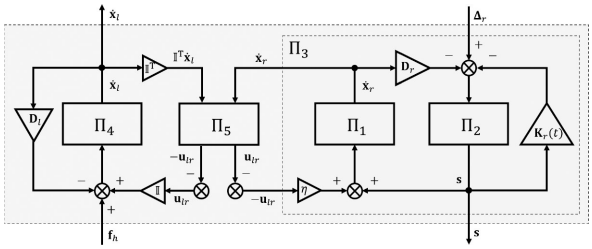

Fig. 3. Schematic representation of the internal power interconnections of the closed-loop bilateral teleoperator with multiple local and remote robots.

In summary, the energy V_3 can be upper-bounded so as to guarantee the tree network connectivity of the RMRS. Because $-\mathbf{u}_{lr}$ is an exogenous input to the system Π_3, the power which it injects into Π_3 needs to be measured and compensated by an excess of output passivity of Π_1. A particular challenge is that $-\mathbf{u}_{lr}$ depends on the distances of the leader remote robots to their associated local robots. Dynamically updated damping could dissipate the energy injected into Π_3 via the port $(-\mathbf{u}_{lr}, \dot{\mathbf{x}}_r)$, but the power-preserving interconnection of Π_1 and Π_2 [see in Fig. 2(a)] prohibits such an update. Therefore, the proposed controller saturates the couplings $\boldsymbol{\theta}_{lri}$ between the local and the leader remote robots to $\overline{\mathbf{f}}_{hi}$ in (3). This coupling saturation limits the power injected into Π_3 through the port $(-\mathbf{u}_{lr}, \dot{\mathbf{x}}_r)$ as in (19) and further in (21) and permits to upper bound the energy V_3 of Π_3 to guarantee the tree connectivity of the RMRS with constant damping injection as in Lemma 1. Because any connected network has a spanning tree, the proposed control paves the way for future work on global connectivity maintenance with switching spanning trees.

3) Closed-Loop Passivity: This section develops a dynamic feedback passivation strategy for the multiuser teleoperation of an RMRS with connectivity maintained as above. The energy behaviors of the local robots and of the couplings between the local and the remote robots guide the proposed modulation of the couplings between, and the damping injection at, the remote robots.

Let the storage of the local robots Π_4 in (10) be quantified by the following weighted sum of kinetic energies:

$$V_4 = \frac{\eta}{2} \dot{\mathbf{x}}_l^{\mathsf{T}} \mathbf{M}_l(\mathbf{x}_l) \dot{\mathbf{x}}_l. \tag{25}$$

The time derivative of V_4 along the dynamics (10) of the local robots

$$\dot{V}_4 = \eta \dot{\mathbf{x}}_l^{\mathsf{T}} \mathbf{f}_h + \eta \dot{\mathbf{x}}_l^{\mathsf{T}} \mathbb{I} \mathbf{u}_{lr} - \eta \dot{\mathbf{x}}_l^{\mathsf{T}} \mathbf{D}_l \dot{\mathbf{x}}_l \tag{26}$$

shows that Π_4 is output strictly passive with the input $\mathbf{f}_h + \mathbb{I}\mathbf{u}_{lr}$ and the output $\dot{\mathbf{x}}_l$ [see Fig. 2(b)].

The controllers (9) and (6) interconnect the local and the remote robots through the inputs $-\eta \mathbf{u}_{lr}$ to Π_1 in (4) and $\mathbb{I}\mathbf{u}_{lr}$ to Π_4 in (10). Modeling them as a two-port coupling network Π_5 with the power ports $(\dot{\mathbf{x}}_r, \mathbf{u}_{lr})$ and $(\mathbb{I}^{\mathsf{T}}\dot{\mathbf{x}}_l, -\mathbf{u}_{lr})$ (see Fig. 3), the

energy of Π_5 can then be quantified by

$$V_5 = \eta \sum_{i=1}^{N_l} \int_{\mathbf{0}}^{\mathbf{x}_{lri}} \tanh\left(K_{lri}\boldsymbol{\delta}\right)^{\mathsf{T}} \overline{\mathbf{F}}_{hi} d\boldsymbol{\delta} \tag{27}$$

which is a positive-definite function of $(\mathbf{x}_{lr1}^{\mathsf{T}}, \ldots, \mathbf{x}_{lrN_l}^{\mathsf{T}})^{\mathsf{T}}$ as $\tanh(\cdot)$ is strictly increasing and odd. The derivative of V_5, i.e.,

$$\dot{V}_5 = \eta \sum_{i=1}^{N_l} \boldsymbol{\theta}_{lri}^{\mathsf{T}} \left(\dot{\mathbf{x}}_{ri} - \dot{\mathbf{x}}_{li}\right) = \eta \mathbf{u}_{lr}^{\mathsf{T}} \dot{\mathbf{x}}_r - \eta \mathbf{u}_{lr}^{\mathsf{T}} \mathbb{I}^{\mathsf{T}} \dot{\mathbf{x}}_l \tag{28}$$

shows that the two-port network Π_5 is passive (lossless) with the inputs $(\dot{\mathbf{x}}_r^{\mathsf{T}}\ \dot{\mathbf{x}}_l^{\mathsf{T}}\mathbb{I})^{\mathsf{T}}$ and the outputs $(\mathbf{u}_{lr}^{\mathsf{T}}\ -\mathbf{u}_{lr}^{\mathsf{T}})^{\mathsf{T}}$.

Then, the two-port network obtained by interconnecting Π_3, Π_4, and Π_5 in Fig. 3 models the bilateral teleoperator with multiple local and remote robots. Its power port $(\mathbf{f}_h, \dot{\mathbf{x}}_l)$ is for physical interaction, and hence for energy exchange, with human users. Given Assumption A1, the bilteral multiuser teleoperation of the RMRS will be rendered stable by making the teleoperator passive with respect to $(\mathbf{f}_h, \dot{\mathbf{x}}_l)$. To this end, the energy potentially injected by $\boldsymbol{\Delta}_r$ will be dissipated by dynamic feedback passivation.

Let the storage function of the teleoperator be

$$V = (V_1 + V_2) + V_4 + V_5 = V_3 + V_4 + V_5 \tag{29}$$

where V_is are the storage functions of the networks Π_i, $i = 1, \ldots, 5$. After adding (16), (26), and (28), its time derivative becomes

$$\begin{aligned} \dot{V} = {} & \eta \dot{\mathbf{x}}_l^{\mathsf{T}} \mathbf{f}_h + \mathbf{s}^{\mathsf{T}} \mathbf{D}_r^{-1} \boldsymbol{\Delta}_r \\ & - \eta \dot{\mathbf{x}}_l^{\mathsf{T}} \mathbf{D}_l \dot{\mathbf{x}}_l - \dot{\mathbf{x}}_r^{\mathsf{T}} \dot{\mathbf{x}}_r - \mathbf{s}^{\mathsf{T}} \mathbf{D}_r^{-1} \mathbf{K}_r(t) \mathbf{s} \end{aligned} \tag{30}$$

where $-\eta \dot{\mathbf{x}}_r^{\mathsf{T}} \mathbf{u}_{lr} + \eta \dot{\mathbf{x}}_l^{\mathsf{T}} \mathbb{I} \mathbf{u}_{lr} + \eta \mathbf{u}_{lr}^{\mathsf{T}} \dot{\mathbf{x}}_r - \eta \mathbf{u}_{lr}^{\mathsf{T}} \mathbb{I}^{\mathsf{T}} \dot{\mathbf{x}}_l = 0$ confirms that the interconnection of Π_1 and Π_4 through Π_5 is power-preserving. Furthermore, $\dot{V}$ demonstrates that the overall teleoperator is output strictly passive with the inputs $\mathbf{f}_h$ and $\boldsymbol{\Delta}_r$ and the outputs $\dot{\mathbf{x}}_l$, $\dot{\mathbf{x}}_r$, and $\mathbf{s}$, with the output passivity index determined by the control gains $\mathbf{D}_l$, $\mathbf{D}_r$, and $\mathbf{K}_r(t)$.

However, the energy injected by the uncertainty $\boldsymbol{\Delta}_r$ may be unbounded. Because $\boldsymbol{\Delta}_r$ in (7) is a function of the states of the system, the possible lack of passivity induced by $\boldsymbol{\Delta}_r$ can be approximated by (see [67, Appendix B])

$$\mathbf{s}^{\mathsf{T}} \mathbf{D}_r^{-1} \boldsymbol{\Delta}_r \leq \eta \dot{\mathbf{x}}_l^{\mathsf{T}} \mathbb{D}_r \dot{\mathbf{x}}_l + \mathbf{1}_{N_r n}^{\mathsf{T}} \mathbf{D}_r^{-1} \mathbf{R} \dot{\mathbf{x}}_r^2 + \mathbf{s}^{\mathsf{T}} \mathbf{D}_r^{-1} \boldsymbol{\Gamma}_1^p(t) \mathbf{s} \tag{31}$$

where $\mathbb{D}_r = \mathbb{I} \mathbf{D}_r^{-1} \mathbb{I}^{\mathsf{T}}$, $\mathbf{R} = 2\eta \mathbb{I}^{\mathsf{T}} \mathbb{I} + \sigma(3\mathbf{D} + 2\mathbf{A}) \otimes \mathbf{I}_n$, and $\boldsymbol{\Gamma}_1^p(t) = \eta \mathbb{I}^{\mathsf{T}} \boldsymbol{\Gamma}_{lr}^p(t) \mathbb{I} + \sigma \boldsymbol{\Gamma}_{rr}(t)$ is a function of the states of the system that entails dynamic feedback passivation. The inequality (31) suggests to rectify the potentially detrimental perturbation $\boldsymbol{\Delta}_r$ through the surplus of output passivity. Using (31), the supply rate (30) can be further bounded by

$$\dot{V} \leq \eta \dot{\mathbf{x}}_l^{\mathsf{T}} \mathbf{f}_h - \dot{\mathbf{x}}_l^{\mathsf{T}} \widehat{\mathbf{D}}_{pl} \dot{\mathbf{x}}_l - \mathbf{1}_{N_r n}^{\mathsf{T}} \widehat{\mathbf{D}}_{pr} \dot{\mathbf{x}}_r^2 - \mathbf{s}^{\mathsf{T}} \widehat{\mathbf{K}}_{pr}(t) \mathbf{s} \tag{32}$$

where $\widehat{\mathbf{D}}_{pl} = \eta(\mathbf{D}_l - \mathbb{D}_r)$ and $\widehat{\mathbf{D}}_{pr} = \mathbf{D}_r^{-1}(\mathbf{D}_r - \mathbf{R})$ are constant, and $\widehat{\mathbf{K}}_{pr}(t) = \mathbf{D}_r^{-1}[\mathbf{K}_r(t) - \boldsymbol{\Gamma}_1^p(t)]$ is state-dependent. Therefore, the dynamic feedback can make the teleoperator passive. The following lemma explicitly formulates the selection and the update of the control gains.

Lemma 2: Consider the teleoperator with multiple local (1) and remote (2) robots under the control of (9) and (6). Let D_{li} and D_{ri} be set and $K_{ri}(t)$ be updated to obey the conditions in Lemma 1 and to make $\widehat{\mathbf{D}}_{pl} \succeq \mathbf{0}$, $\widehat{\mathbf{D}}_{pr} \mathbf{1}_{N_r n} \geq \mathbf{0}$, and $\widehat{\mathbf{K}}_{pr}(t) \succeq \mathbf{0}$.

Then, the teleoperator is passive with respect to the power port $(\mathbf{f}_h, \dot{\mathbf{x}}_l)$. Furthermore, if $\widehat{\mathbf{D}}_{pl} \succ \mathbf{0}$, $\widehat{\mathbf{D}}_{pr} \mathbf{1}_{N_r n} > \mathbf{0}$, and $\widehat{\mathbf{K}}_{pr}(t) \succ \mathbf{0}$, then $\dot{\mathbf{x}}_l$, $\dot{\mathbf{x}}_r$, and $\mathbf{s}$ are square integrable.

Proof: The conditions in Lemma 1 guarantee the tree network connectivity of the RMRS. Then, if $\widehat{\mathbf{D}}_{pl} \succeq \mathbf{0}$, $\widehat{\mathbf{D}}_{pr} \mathbf{1}_{N_r n} \geq \mathbf{0}$, and $\widehat{\mathbf{K}}_{pr}(t) \succeq \mathbf{0}$, the passivity of the teleoperator can be directly concluded from (32). Furthermore, if $\widehat{\mathbf{D}}_{pl} \succ \mathbf{0}$, $\widehat{\mathbf{D}}_{pr} \mathbf{1}_{N_r n} > \mathbf{0}$, and $\widehat{\mathbf{K}}_{pr}(t) \succ \mathbf{0}$, then there exists $k > 0$ such that $\dot{V} \leq \eta \dot{\mathbf{x}}_l^{\mathsf{T}} \mathbf{f}_h - k(\dot{\mathbf{x}}_l^{\mathsf{T}} \dot{\mathbf{x}}_l + \dot{\mathbf{x}}_r^{\mathsf{T}} \dot{\mathbf{x}}_r + \mathbf{s}^{\mathsf{T}} \mathbf{s})$. The time integration of $\dot{V}$ then leads to $k \int_0^t \|\dot{\mathbf{x}}_l(\tau)\|^2 d\tau + k \int_0^t \|\dot{\mathbf{x}}_r(\tau)\|^2 d\tau + k \int_0^t \|\mathbf{s}(\tau)\|^2 d\tau \leq V(0) - V(t) + \eta \int_0^t \dot{\mathbf{x}}_l^{\mathsf{T}}(\tau) \mathbf{f}_h(\tau) d\tau$, and, together with $V(t) \geq 0$ and Assumption A1, proves that $\dot{\mathbf{x}}_l$, $\dot{\mathbf{x}}_r$, and $\mathbf{s}$ are square integrable. ■

The bilateral teleoperator with multiple local and remote robots is a networked robotic system in physical interaction with its multiple human operators through the power-preserving ports $(\mathbf{f}_{hi}, \dot{\mathbf{x}}_{li})$. Since a power-preserving interconnection of passive components yields a passive system, this article assumes passive human operators (see Assumption A1) and passivates the teleoperator to guarantee stable multiuser teleoperation of an RMRS with tree connectivity.

To the bilateral teleoperator, the user forces $\mathbf{f}_{hi}$ are the inputs that it transmits to the RMRS through the couplings of the leader remote robots to the local robots. In return, the teleoperator feeds haptic cues back to the users through the couplings of the local robots to the leader remote robots. Those haptic cues may convey unwanted fluctuations of the RMRS. More importantly, inappropriate couplings between the remote robots may amplify unfavorable motion deviations of the local robots and jeopardize the safety of the system [62].

To eliminate the reflection-induced instability, this section renders the teleoperator passive. It designs a dynamic feedback passivation strategy that modulates the couplings and damping injection throughout the teleoperator based on the distances between, and the velocities of, the robots. Intuitively, the RMRS collectively behaves like a deformable multinodal object interacting with the multiple local robots: the local robots are linked to their associated leader remote robots by the saturated proportional $(\boldsymbol{\theta}_{lri})$ plus damping $(-D_{li}\dot{\mathbf{x}}_{li})$ control (9), while the RMRS adaptively tracks the local robots using the dynamic controllers (6). Typically, $\eta K_{ri}(t) \neq 1$ and the couplings between the local and the remote robots are time-varying and asymmetric. Furthermore, the control inputs $-\sigma K_{ri}(t) \boldsymbol{\theta}_{ri}$ in $\mathbf{f}_{ri}$ of the remote robots imply that the couplings between the remote robots are also dynamically adjusted, based on their distances to their neighbors. Nonetheless, selecting the control gains as in Lemma 2 provably renders the teleoperator passive with respect to its power port $(\mathbf{f}_h, \dot{\mathbf{x}}_l)$.

Because the RMRS (2) is in free motion, the teleoperator exchanges energy only with its human users via the power

ports $(\mathbf{f}_{hi}, \dot{\mathbf{x}}_{li})$, and Assumption A1 and Lemma 2 guarantee the closed-loop stability of the bilateral teleoperation. The stable teleoperation of an RMRS in physical interaction with the environment remains a challenge. Early research preserves the local [65] and the global [63] connectivity of the RMRS by deriving the couplings between the remote robots from unbounded potentials. Those couplings grow infinite when the inter-robot distances approach the communication radius. Therefore, the designs based on unbounded potentials can become numerically unstable and are sensitive to noise in practical implementation. This article circumvents the numerical instability by embedding the gradient of a bounded potential into the sliding variable $\mathbf{s}_i$ and converting the dynamics (2) of the RMRS into (5), but cannot guarantee passive interactions between the remote robots and the environment. Future research will investigate how to update the coupling and damping gains of the RMRS to render the teleoperator passive with respect to the power ports $(\mathbf{f}_{ei}, \dot{\mathbf{x}}_{ri})$, where $\mathbf{f}_{ei}$ are the environment forces applied to the remote robots $i = 1, \ldots, N_r$.

B. Teleoperation With Delays

A bilateral multiuser-multirobot teleoperation system can have delayed communications both between the local and the remote robots and between the remote robots. In a first step toward overcoming the delay-induced challenges, this section extends the feedback passivation strategy in Section IV-A to cope with time-delayed communications between the local and the remote robots.

1) Control as Interconnection: In Section IV-A, the sliding variables $\mathbf{s}_i$ designed in (3) split the dynamics of the RMRS into two dynamical systems Π_1 and Π_2 that are negatively feedback interconnected. The resulting dynamical system Π_3 is consistently perturbed by the uncertainty $\boldsymbol{\Delta}_r$, in which $\boldsymbol{\Delta}_{lri}$ is injected by the interconnections $\boldsymbol{\theta}_{lri}$ between the local and the remote robots. To preserve the connectivity of the RMRS and to ensure the passivity of the bilateral teleoperator, the control gains $\mathbf{K}_r(t)$ of the leader remote robots are updated as in Lemmas 1 and 2, using the transmitted positions and velocities of the local robots. Yet, time-varying communication delays between the local robots and the leader remote robots may thwart the adaptation of $\mathbf{K}_r(t)$. Hereafter, their harmful effect is overcome by insulating $\boldsymbol{\Delta}_r$ from the local side via appropriate couplings between the local and the remote robots.

Endow every leader remote robot i with an auxiliary variable $\boldsymbol{\xi}_i \in \mathbb{R}^n$ that evolves with

$$\dot{\boldsymbol{\xi}}_i = K_{lci}(\mathbf{x}_{lid} - \boldsymbol{\xi}_i) + \boldsymbol{\theta}_{cri} \tag{33}$$

where $i = 1, \ldots, N_l$, $K_{lci} > 0$, $\mathbf{x}_{lid} = \mathbf{x}_{li}(t - T_{li}(t))$ is the position of the local robot i delayed by $T_{li}(t)$, and

$$\boldsymbol{\theta}_{cri} = \overline{\mathbf{F}}_{hi} \cdot \tanh\left[K_{cri}(\mathbf{x}_{ri} - \boldsymbol{\xi}_i)\right]$$

with $K_{cri} > 0$. Furthermore, reconstruct the sliding variable $\mathbf{s}_i$ of *each leader* remote robot $i = 1, \ldots, N_l$ by

$$\mathbf{s}_i = \dot{\mathbf{x}}_{ri} + \sigma\boldsymbol{\theta}_{ri} + \eta\boldsymbol{\theta}_{cri} \tag{34}$$

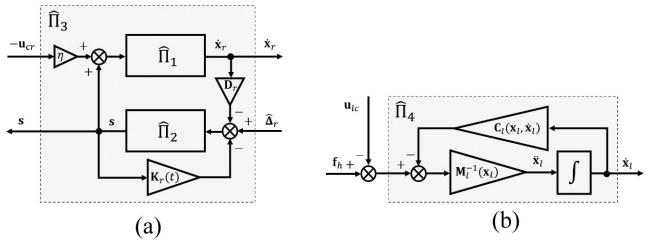

Fig. 4. Input–output diagrams (a) of the RMRS $\widehat{\Pi}_3$ (the feedback interconnection of $\widehat{\Pi}_1$ and $\widehat{\Pi}_2$) and (b) of the local robots $\widehat{\Pi}_4$.

and rearrange the dynamics of *all* remote robots (2) into

$$\mathbf{M}_{ri}(\mathbf{x}_{ri})\dot{\mathbf{s}}_i + \mathbf{C}_{ri}(\mathbf{x}_{ri}, \dot{\mathbf{x}}_{ri})\mathbf{s}_i = \sigma\boldsymbol{\Delta}_{rri} + \eta\boldsymbol{\Delta}_{cri} + \mathbf{f}_{ri} \tag{35}$$

where $i = 1, \ldots, N_r$, $\boldsymbol{\Delta}_{rri}$ are defined in (5), and

$$\boldsymbol{\Delta}_{cri} = \begin{cases} \mathbf{M}_{ri}(\mathbf{x}_{ri})\dot{\boldsymbol{\theta}}_{cri} + \mathbf{C}_{ri}(\mathbf{x}_{ri}, \dot{\mathbf{x}}_{ri})\boldsymbol{\theta}_{cri}, & i = 1, \ldots, N_l \\ \mathbf{0}, & \text{otherwise} \end{cases}.$$

Then, as in Section IV-A1, the dynamics $\widehat{\Pi}_3$ of the RMRS under the control of (6) can be cast into a feedback interconnection of

$$\widehat{\Pi}_1: \quad \dot{\mathbf{x}}_r = -\sigma\left[\mathbf{L}(\mathbf{x}_r) \otimes \mathbf{I}_n\right]\mathbf{x}_r + \mathbf{s} - \eta\mathbf{u}_{cr} \tag{36}$$

and the transformed dynamics of the RMRS

$$\widehat{\Pi}_2: \quad \mathbf{M}_r(\mathbf{x}_r)\dot{\mathbf{s}} + \mathbf{C}_r(\mathbf{x}_r, \dot{\mathbf{x}}_r)\mathbf{s} = \widehat{\boldsymbol{\Delta}}_r - \mathbf{K}_r(t)\mathbf{s} - \mathbf{D}_r\dot{\mathbf{x}}_r \tag{37}$$

where $\mathbf{u}_{cr} = (\boldsymbol{\theta}_{cr1}^{\mathsf{T}}, \ldots, \boldsymbol{\theta}_{crN_l}^{\mathsf{T}}, \mathbf{0}^{\mathsf{T}}, \ldots, \mathbf{0}^{\mathsf{T}})^{\mathsf{T}}$ and $\widehat{\boldsymbol{\Delta}}_r = (\sigma\boldsymbol{\Delta}_{rr1}^{\mathsf{T}} + \eta\boldsymbol{\Delta}_{cr1}^{\mathsf{T}}, \ldots, \sigma\boldsymbol{\Delta}_{rrN_r}^{\mathsf{T}} + \eta\boldsymbol{\Delta}_{crN_r}^{\mathsf{T}})^{\mathsf{T}}$ [see Fig. 4(a)].

Force feedback is rendered to every operator i by connecting their local robot i to the associated leader remote robot i via

$$\mathbf{f}_{li} = K_{lci}(\boldsymbol{\xi}_{id} - \mathbf{x}_{li}) - D_{li}\dot{\mathbf{x}}_{li} \tag{38}$$

where $\boldsymbol{\xi}_{id} = \boldsymbol{\xi}_i(t - T_{ri}(t))$ arrives at the local robot i at time t with delay $T_{ri}(t)$. Then, the local robot dynamics $\widehat{\Pi}_4$ become

$$\widehat{\Pi}_4: \quad \mathbf{M}_l(\mathbf{x}_l)\ddot{\mathbf{x}}_l + \mathbf{C}_l(\mathbf{x}_l, \dot{\mathbf{x}}_l)\dot{\mathbf{x}}_l = \mathbf{f}_h - \mathbf{u}_{lc} \tag{39}$$

where the input $\mathbf{u}_{lc} = \mathbf{D}_l\dot{\mathbf{x}}_l - \mathbf{u}_{lcd}$ with $\mathbf{u}_{lcd} = \mathbf{K}_{lc}(\boldsymbol{\xi}_d - \mathbf{x}_l)$, $\mathbf{K}_{lc} = \mathrm{Diag}\{K_{lci}\mathbf{I}_n\}$, and $\boldsymbol{\xi}_d = (\boldsymbol{\xi}_{1d}^{\mathsf{T}}, \ldots, \boldsymbol{\xi}_{N_l d}^{\mathsf{T}})^{\mathsf{T}}$. Unlike Fig. 2(b), Fig. 4(b) depicts the damping injection $-\mathbf{D}_l\dot{\mathbf{x}}_l$ as an input to the local robot dynamics $\widehat{\Pi}_4$. This treatment of the injected damping is key to passivating the time-delayed interconnections between the local and the remote robots next.

Let $\boldsymbol{\xi} = (\boldsymbol{\xi}_1^{\mathsf{T}}, \ldots, \boldsymbol{\xi}_{N_l}^{\mathsf{T}})^{\mathsf{T}}$ and group the dynamics (33) of the auxiliary variables $\boldsymbol{\xi}_i$ into

$$\dot{\boldsymbol{\xi}} = \mathbf{u}_{ldc} + \mathbb{I}\mathbf{u}_{cr} \tag{40}$$

where $\mathbf{u}_{ldc} = \mathbf{K}_{lc}(\mathbf{x}_{ld} - \boldsymbol{\xi})$ depends on the time-delayed positions $\mathbf{x}_{ld} = (\mathbf{x}_{l1d}^{\mathsf{T}}, \ldots, \mathbf{x}_{lN_l d}^{\mathsf{T}})^{\mathsf{T}}$ of the local robots. The teleoperator can then be modeled as in Fig. 5, where the shaded region groups the dynamics $\widehat{\Pi}_c$ of the time-delayed interconnections between the local and the remote robots. Note that $\widehat{\Pi}_c$ includes the damping injection $-\mathbf{D}_l\dot{\mathbf{x}}_l$ on the local side and the auxiliary dynamics (40) on the remote side, to facilitate the passivation of those interconnections in this section. Note also that $\widehat{\Pi}_5$ and $\widehat{\Pi}_6$ have integrator-type dynamics: $\widehat{\Pi}_5$ is a nonlinear single

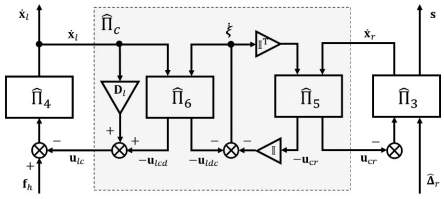

Fig. 5. Input–output dynamic interconnections of the bilateral teleoperator with time-delayed communications between the local and the remote robots.

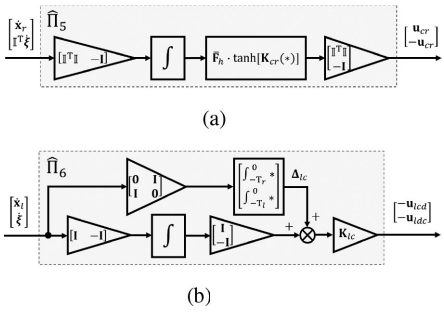

Fig. 6. Subsystems $\widehat{\Pi}_5$ and $\widehat{\Pi}_6$ of $\widehat{\Pi}_c$ (the system of the time-delayed couplings between the local and the remote robots) in Fig. 5. (a) Subsystem $\widehat{\Pi}_5$ is a nonlinear integrator. (b) Subsystem $\widehat{\Pi}_6$ combines a linear integrator with the delay-induced uncertain dynamics $\boldsymbol{\Delta}_{lc}$.

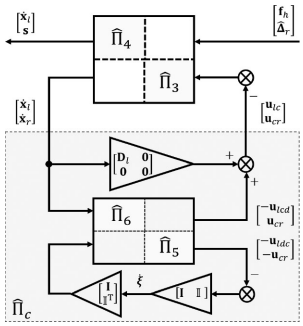

Fig. 7. Controlled teleoperator as a power-conserving interconnection of a nonpassive physical component with a passive cyber component.

integrator with the inputs $[\dot{\mathbf{x}}_r\ (\mathbb{I}^\mathsf{T}\dot{\boldsymbol{\xi}})]$ and the outputs $[\mathbf{u}_{cr}\ -\mathbf{u}_{cr}]$, as shown in Fig. 6(a); in contrast, $\widehat{\Pi}_6$ has the inputs $[\dot{\mathbf{x}}_l\ \dot{\boldsymbol{\xi}}]$ and the outputs $[-\mathbf{u}_{lcd}\ -\mathbf{u}_{ldc}]$ and includes, besides a linear single integrator, the uncertain dynamics $\boldsymbol{\Delta}_{lc} = (\boldsymbol{\xi}^\mathsf{T} - \boldsymbol{\xi}_d^\mathsf{T},\ \mathbf{x}_l^\mathsf{T} - \mathbf{x}_{ld}^\mathsf{T})^\mathsf{T}$ induced by the time-varying delays [see Fig. 6(b)].

Grouping $\widehat{\Pi}_3$ and $\widehat{\Pi}_4$ into a physical component and $\widehat{\Pi}_5$ and $\widehat{\Pi}_6$ into a cyber component permits to reorganize the teleoperator in Fig. 5 as in Fig. 7. The physical component therein is the block diagonalization of the dynamics $\widehat{\Pi}_4$ and $\widehat{\Pi}_3$ and has two input–output pairs: $([\mathbf{f}_h\ \widehat{\boldsymbol{\Delta}}_r], [\dot{\mathbf{x}}_l\ \mathbf{s}])$ and $(-[\mathbf{u}_{lc}\ \mathbf{u}_{cr}], [\dot{\mathbf{x}}_l\ \dot{\mathbf{x}}_r])$. The first pair of the inputs $[\mathbf{f}_h\ \widehat{\boldsymbol{\Delta}}_r]$ and the outputs $[\dot{\mathbf{x}}_l\ \mathbf{s}]$ comprises the power port $(\mathbf{f}_h, \dot{\mathbf{x}}_l)$ reserved for physical interaction, and hence for exchange of energy, with the human users, and the power port $(\widehat{\boldsymbol{\Delta}}_r, \mathbf{s})$ to be damped by internal feedback passivation for connectivity maintenance and by external energy dissipation for closed-loop passivity. The second pair of the inputs $-[\mathbf{u}_{lc}\ \mathbf{u}_{cr}]$ and the outputs $[\dot{\mathbf{x}}_l\ \dot{\mathbf{x}}_r]$ is the power-preserving interconnection with the cyber component $\widehat{\Pi}_c$.

The cyber component $\widehat{\Pi}_c$ of the teleoperator consists of a block diagonalization of the dynamics $\widehat{\Pi}_5$ and $\widehat{\Pi}_6$. It couples the local and remote sides and comprises the delay-induced uncertain dynamics $\boldsymbol{\Delta}_{lc}$ in $\widehat{\Pi}_6$. The feedforward damping injection on the local side and the feedback auxiliary dynamics $\dot{\boldsymbol{\xi}}$ on the remote side render the cyber component passive. Note the "control as interconnection" paradigm of the proposed strategy: a power-preserving interconnection of a nonpassive physical component with a passive cyber component.

2) Connectivity and Passivity: Similar to Section IV-A, this section first maintains the tree connectivity of the RMRS without assuming a passive teleoperator. It then renders passive a teleoperator whose RMRS is connected.

At the RMRS side, $\widehat{\Pi}_3$ is the feedback interconnection of $\widehat{\Pi}_1$ and $\widehat{\Pi}_2$. In turn, $\widehat{\Pi}_1$ and $\widehat{\Pi}_2$ are analogous to Π_1 and Π_2. Then, V_3 in (15) can measure the energy of $\widehat{\Pi}_3$. Its derivative along the dynamics (36) and (37) is

$$\dot{V}_3 = \mathbf{s}^\mathsf{T}\mathbf{D}_r^{-1}\widehat{\boldsymbol{\Delta}}_r - \eta\dot{\mathbf{x}}_r^\mathsf{T}\mathbf{u}_{cr} - \dot{\mathbf{x}}_r^\mathsf{T}\dot{\mathbf{x}}_r - \mathbf{s}^\mathsf{T}\mathbf{D}_r^{-1}\mathbf{K}_r(t)\mathbf{s}. \quad (41)$$

[67, Appendix C] shows that $\widehat{\boldsymbol{\Delta}}_r$ injects power bounded by

$$\mathbf{s}^\mathsf{T}\mathbf{D}_r^{-1}\widehat{\boldsymbol{\Delta}}_r \le \mathbf{1}_{N_r n}^\mathsf{T}\mathbf{D}_r^{-1}\left[\eta\mathbb{I}^\mathsf{T}\mathbb{I} + \sigma(3\mathbf{D}+2\mathbf{A})\otimes\mathbf{I}_n\right]\dot{\mathbf{x}}_r^2 + \mathbf{s}^\mathsf{T}\mathbf{D}_r^{-1}\boldsymbol{\Gamma}_2^c(t)\mathbf{s} + \eta^2\overline{\mathbf{f}}_h^\mathsf{T}\mathbb{I}\mathbf{D}_r^{-1}\mathbb{I}^\mathsf{T}\overline{\mathbf{f}}_h \quad (42)$$

with $\boldsymbol{\Gamma}_2^c(t) = \eta\mathbb{I}^\mathsf{T}\boldsymbol{\Gamma}_{cr}^c(t)\mathbb{I} + \sigma\boldsymbol{\Gamma}_{rr}(t)$, and the RMRS $\widehat{\Pi}_3$ extracts the maximum power

$$-\eta\dot{\mathbf{x}}_r^\mathsf{T}\mathbf{u}_{cr} \le \dot{\mathbf{x}}_r^\mathsf{T}\dot{\mathbf{x}}_r/4 + \eta^2\mathbf{u}_{cr}^\mathsf{T}\mathbf{u}_{cr} \quad (43)$$

from the couplings $\widehat{\Pi}_c$ between the local and the remote robots. Similar to (18), the input $-\mathbf{u}_{cr}$, the outputs $\dot{\mathbf{x}}_r$, and the auxiliary variables $\mathbf{s}$ of the RMRS determine an upper bound on the energy V_3 of $\widehat{\Pi}_3$ as follows:

$$V_3 \le \frac{k_r}{2\sigma\lambda_L}\left(2\dot{\mathbf{x}}_r^\mathsf{T}\dot{\mathbf{x}}_r + 2\mathbf{s}^\mathsf{T}\mathbf{s} + \eta^2\mathbf{u}_{cr}^\mathsf{T}\mathbf{u}_{cr}\right) + \frac{1}{2}\mathbf{s}^\mathsf{T}\mathbf{D}_r^{-1}\boldsymbol{\Lambda}_r\mathbf{s}. \quad (44)$$

Equations (42)–(44) then lead to an upper bound on the time derivative (41) of V_3:

$$\dot{V}_3 \le \frac{\eta^2}{8}\overline{\mathbf{f}}_h^\mathsf{T}\mathbb{I}\left(9\mathbf{I}_{N_r n} + 8\mathbf{D}_r^{-1}\right)\mathbb{I}^\mathsf{T}\overline{\mathbf{f}}_h - \frac{\sigma\lambda_L}{4k_r}V_3 - \frac{1}{2}\mathbf{1}_{N_r n}^\mathsf{T}\mathbf{D}_r^{-1}\widehat{\mathbf{D}}_{cr}\dot{\mathbf{x}}_r^2 - \mathbf{s}^\mathsf{T}\mathbf{D}_r^{-1}\widehat{\mathbf{K}}_{cr}(t)\mathbf{s} \quad (45)$$

where $\mathbf{u}_{cr}^\mathsf{T}\mathbf{u}_{cr} \le \overline{\mathbf{f}}_h^\mathsf{T}\mathbb{I}\mathbb{I}^\mathsf{T}\overline{\mathbf{f}}_h$ has been used, and

$$\widehat{\mathbf{D}}_{cr} = \mathbf{D}_r - 2\eta\mathbb{I}^\mathsf{T}\mathbb{I} - 2\sigma(3\mathbf{D}+2\mathbf{A})\otimes\mathbf{I}_n$$

$$\widehat{\mathbf{K}}_{cr}(t) = \mathbf{K}_r(t) - (\sigma\lambda_L\boldsymbol{\Lambda}_r + 2k_r\mathbf{D}_r)/(8k_r) - \boldsymbol{\Gamma}_2^c(t).$$

The strong similarity between (45) and (21) is expected because $\widehat{\Pi}_1$ and $\widehat{\Pi}_2$ have the same input–output properties and the same feedback interconnection in $\widehat{\Pi}_3$ as Π_1 and Π_2 have in Π_3. With the inputs $[-\mathbf{u}_{lr}\ \boldsymbol{\Delta}_r]$ to Π_3 replaced by the inputs $[-\mathbf{u}_{cr}\ \widehat{\boldsymbol{\Delta}}_r]$ to $\widehat{\Pi}_3$, the control gains $\mathbf{K}_r(t)$ of the leader remote robots need to be updated online to make $\widehat{\mathbf{K}}_{cr}(t)$ rather than $\mathbf{K}_{cr}(t)$ positive semidefinite, and thus to preserve the tree communication network of the RMRS, in the presence of

time-delayed communications between the local and the remote robots. More specifically, the auxiliary dynamics (40) at the leader remote robots eliminate the need for information about the local robots when updating $\mathbf{K}_r(t)$ to maintain connectivity.

The following lemma summarizes the conditions for preserving the tree connectivity of an RMRS connected to the local robots over time-delayed communications. The proof is omitted to save space.

Lemma 3: Consider the RMRS (2) with the control (6). Let the auxiliary variables $\boldsymbol{\xi}_i$ have the dynamics (33) and the sliding variables $\mathbf{s}_i$ be redefined in (34) for all the leader remote robots. Also, let D_{ri} be selected and $K_{ri}(t)$ be updated to make $\mathbf{D}_r^{-1}\widehat{\mathbf{D}}_{cr}\mathbf{1}_{N_r n} \geq \mathbf{0}$ and $\widehat{\mathbf{K}}_{cr}(t) \succeq \mathbf{0}$ and to satisfy (22).

Then, the tree communication network of the RMRS remains invariant, i.e., $\mathcal{E}(t) = \mathcal{E}(0),\ \forall t \geq 0$.

Consider the teleoperator with dynamics recast as in Fig. 7 and with the connectivity of the RMRS preserved as in Lemma 3. Its passivity can be inferred from the passivity of its two components: the physical component (the local and the remote robots, or the plant) and the cyber component (the couplings between the local and the remote robots plus the damping of the local robots, or the dynamic controller $\widehat{\Pi}_c$).

Let V_4 in (25) be the energy of the local robots $\widehat{\Pi}_4$, and

$$\widehat{V}_p = V_3 + V_4 \tag{46}$$

be the energy of the plant. By [67, Appendix D], the uncertain dynamics $\widehat{\boldsymbol{\Delta}}_r$ may cause a shortage of passivity of the plant by

$$\mathbf{s}^{\mathsf{T}}\mathbf{D}_r^{-1}\widehat{\boldsymbol{\Delta}}_r \leq \eta\dot{\boldsymbol{\xi}}^{\mathsf{T}}\mathbb{D}_r\dot{\boldsymbol{\xi}} + \mathbf{1}_{N_r n}^{\mathsf{T}}\mathbf{D}_r^{-1}\mathbf{R}\dot{\mathbf{x}}_r^2 + \mathbf{s}^{\mathsf{T}}\mathbf{D}_r^{-1}\boldsymbol{\Gamma}_2^p(t)\mathbf{s} \tag{47}$$

where $\mathbb{D}_r$ and $\mathbf{R}$ are defined in (31) and $\boldsymbol{\Gamma}_2^p(t) = \eta\mathbb{I}^{\mathsf{T}}\boldsymbol{\Gamma}_{cr}^p(t)\mathbb{I} + \sigma\boldsymbol{\Gamma}_{rr}(t)$. Then, (41), (47), and the derivative of V_4 along (39) lead to

$$\begin{aligned}\dot{\widehat{V}}_p \leq\ & \eta\dot{\mathbf{x}}_l^{\mathsf{T}}\mathbf{f}_h - \eta\left(\dot{\mathbf{x}}_l^{\mathsf{T}}\ \dot{\mathbf{x}}_r^{\mathsf{T}}\right)\left(\mathbf{u}_{lc}^{\mathsf{T}}\ \mathbf{u}_{cr}^{\mathsf{T}}\right)^{\mathsf{T}} \\ & + \eta\dot{\boldsymbol{\xi}}^{\mathsf{T}}\mathbb{D}_r\dot{\boldsymbol{\xi}} - \mathbf{1}_{N_r n}^{\mathsf{T}}\overline{\mathbf{D}}_{pr}\dot{\mathbf{x}}_r^2 - \mathbf{s}^{\mathsf{T}}\overline{\mathbf{K}}_{pr}(t)\mathbf{s}\end{aligned} \tag{48}$$

for $\overline{\mathbf{D}}_{pr} = \mathbf{D}_r^{-1}(\mathbf{D}_r - \mathbf{R})$ and $\overline{\mathbf{K}}_{pr}(t) = \mathbf{D}_r^{-1}[\mathbf{K}_r(t) - \boldsymbol{\Gamma}_2^p(t)]$.

By (48), the physical component exchanges energy with the users via the port $(\mathbf{f}_h, \dot{\mathbf{x}}_l)$, and with the cyber component $\widehat{\Pi}_c$ via the port $(-[\mathbf{u}_{lc}\ \mathbf{u}_{cr}], [\dot{\mathbf{x}}_l\ \dot{\mathbf{x}}_r])$. Given that the feedback passivation control $-\mathbf{K}_r(t)\mathbf{s} - \mathbf{D}_r\dot{\mathbf{x}}_r$ can dissipate only part of the energy potentially injected into $\widehat{\Pi}_3$ through the power port $(\widehat{\boldsymbol{\Delta}}_r, \mathbf{s})$, the controller $\widehat{\Pi}_c$ will be designed to extract sufficient power by $\eta\dot{\boldsymbol{\xi}}^{\mathsf{T}}\mathbb{D}_r\dot{\boldsymbol{\xi}}$ in (48) to make the teleoperator passive. Namely, the excess of passivity of the cyber component $\widehat{\Pi}_c$ will be designed to compensate for the potential lack of passivity of the physical component (the plant). Nonetheless, time-varying delays in the communications between the local and the remote robots can lead to the uncertainty $\boldsymbol{\Delta}_{lc}$ in $\widehat{\Pi}_6$ and, hence, to a nonpassive composition of $\widehat{\Pi}_5$ and $\widehat{\Pi}_6$. The potential shortage of passivity of the cyber component $\widehat{\Pi}_c$ caused by the time-varying delays will be tackled by the damping in feedforward at the local robots and by the auxiliary dynamics $\dot{\boldsymbol{\xi}}$ in feedback at the remote robots.

To evaluate the passivity of the composition of $\widehat{\Pi}_5$ and $\widehat{\Pi}_6$, first quantify the energy of the nonlinear integrator $\widehat{\Pi}_5$ by

$$\widehat{V}_5 = \eta\sum_{i=1}^{N_l}\int_{\mathbf{0}}^{\mathbf{x}_{ri}-\boldsymbol{\xi}_i}\tanh\left(K_{cri}\boldsymbol{\delta}_i\right)^{\mathsf{T}}\overline{\mathbf{F}}_{hi}d\boldsymbol{\delta}_i \tag{49}$$

which is positive definite in $\mathbf{x}_{ri} - \boldsymbol{\xi}_i$ since $\tanh(\cdot)$ is strictly increasing and odd. By $\mathbf{u}_{cr}$ in (36), the derivative of $\widehat{V}_5$ is

$$\dot{\widehat{V}}_5 = \eta\left(\mathbf{u}_{cr}^{\mathsf{T}}\ -\mathbf{u}_{cr}^{\mathsf{T}}\right)\left(\dot{\mathbf{x}}_r^{\mathsf{T}}\ \left(\mathbb{I}^{\mathsf{T}}\dot{\boldsymbol{\xi}}\right)^{\mathsf{T}}\right)^{\mathsf{T}} \tag{50}$$

and indicates that $\widehat{\Pi}_5$ in Fig. 6(a) is passive (lossless) with respect to the inputs $[\dot{\mathbf{x}}_r\ \mathbb{I}^{\mathsf{T}}\dot{\boldsymbol{\xi}}]$ and the outputs $[\mathbf{u}_{cr}\ -\mathbf{u}_{cr}]$. Second, measure the storage of the linear integrator $\widehat{\Pi}_6$ with the delay-induced uncertainty $\boldsymbol{\Delta}_{lc}$ by

$$\widehat{V}_6 = \frac{\eta}{2}(\mathbf{x}_l - \boldsymbol{\xi})^{\mathsf{T}}\mathbf{K}_{lc}(\mathbf{x}_l - \boldsymbol{\xi}) \tag{51}$$

whose time derivative is

$$\dot{\widehat{V}}_6 = -\eta\left(\mathbf{u}_{lcd}^{\mathsf{T}}\ \mathbf{u}_{ldc}^{\mathsf{T}}\right)\left(\dot{\mathbf{x}}_l^{\mathsf{T}}\ \dot{\boldsymbol{\xi}}^{\mathsf{T}}\right)^{\mathsf{T}} - \eta\left(\dot{\mathbf{x}}_l^{\mathsf{T}}\ \dot{\boldsymbol{\xi}}^{\mathsf{T}}\right)(\mathbf{I}_2 \otimes \mathbf{K}_{lc})\,\boldsymbol{\Delta}_{lc}. \tag{52}$$

Then, the energy stored in the connections between the local and the leader remote robots (the composition of $\widehat{\Pi}_5$ and $\widehat{\Pi}_6$) is

$$\widehat{V}_c = \widehat{V}_5 + \widehat{V}_6 \tag{53}$$

and the summation of (50) and (52) leads to its time derivative

$$\begin{aligned}\dot{\widehat{V}}_c = & \eta\left(-\mathbf{u}_{lcd}^{\mathsf{T}}\ \mathbf{u}_{cr}^{\mathsf{T}}\right)\left(\dot{\mathbf{x}}_l^{\mathsf{T}}\ \dot{\mathbf{x}}_r^{\mathsf{T}}\right)^{\mathsf{T}} - \eta\left(\mathbf{u}_{ldc}^{\mathsf{T}}\ \mathbf{u}_{cr}^{\mathsf{T}}\right)\left[\mathbf{I}_{N_l n}\ \mathbb{I}\right]^{\mathsf{T}}\dot{\boldsymbol{\xi}} \\ & - \eta\left(\dot{\mathbf{x}}_l^{\mathsf{T}}\ \dot{\boldsymbol{\xi}}^{\mathsf{T}}\right)(\mathbf{I}_2 \otimes \mathbf{K}_{lc})\,\boldsymbol{\Delta}_{lc}.\end{aligned}$$

The inequality obtained in [67, Appendix E] demonstrates that the potential lack of passivity resulting from the delay-induced uncertain dynamics $\boldsymbol{\Delta}_{lc}$ depends on the input $\dot{\mathbf{x}}_l$ and on the auxiliary dynamics $\dot{\boldsymbol{\xi}}$. This inequality inspires the following passivation strategy: include the damping $-\mathbf{D}_l\dot{\mathbf{x}}_l$ of the local robots as a feedforward loop in $\widehat{\Pi}_c$ to convert the output $-\mathbf{u}_{lcd}$ into $\mathbf{u}_{lc}$ to compensate for the shortage of passivity linked to $\dot{\mathbf{x}}_l$; add a feedback loop inside $\widehat{\Pi}_c$ to connect the outputs $[-\mathbf{u}_{ldc}\ -\mathbf{u}_{cr}]$ to the inputs $[\dot{\boldsymbol{\xi}}\ \mathbb{I}^{\mathsf{T}}\dot{\boldsymbol{\xi}}]$ by the adaptation (40) of $\boldsymbol{\xi}$; and inject adequate dissipation into $\widehat{\Pi}_c$ to balance the lack of passivity both of the cyber component (the couplings between the local and the remote robots) and of the physical component (the local and the remote robots). Thus, the gist in this section is a feedforward–feedback passivation strategy that transforms the couplings between the local and the remote robots into a dynamical controller $\widehat{\Pi}_c$ that is interconnected with the physical component and regulates the passivity margin of the teleoperator.

More specifically, the feedforward loop by $\mathbf{u}_{lc} = \mathbf{D}_l\dot{\mathbf{x}}_l - \mathbf{u}_{lcd}$ in (39) and the feedback loop by $\dot{\boldsymbol{\xi}} = \mathbf{u}_{ldc} + \mathbb{I}\mathbf{u}_{cr}$ in (40) jointly convert $\dot{\widehat{V}}_c$ into

$$\begin{aligned}\dot{\widehat{V}}_c = & \eta\left(\mathbf{u}_{lc}^{\mathsf{T}}\ \mathbf{u}_{cr}^{\mathsf{T}}\right)\left(\dot{\mathbf{x}}_l^{\mathsf{T}}\ \dot{\mathbf{x}}_r^{\mathsf{T}}\right)^{\mathsf{T}} - \eta\left(\dot{\mathbf{x}}_l^{\mathsf{T}}\ \dot{\boldsymbol{\xi}}^{\mathsf{T}}\right)(\mathbf{I}_2 \otimes \mathbf{K}_{lc})\,\boldsymbol{\Delta}_{lc} \\ & - \eta\dot{\mathbf{x}}_l^{\mathsf{T}}\mathbf{D}_l\dot{\mathbf{x}}_l - \eta\dot{\boldsymbol{\xi}}^{\mathsf{T}}\dot{\boldsymbol{\xi}}\end{aligned}$$

from which it follows that

$$\widehat{V}_c(t) \leq \widehat{V}_c(0) + \eta \int_0^t \left(\mathbf{u}_{lc}^{\mathsf{T}}(\tau)\ \mathbf{u}_{cr}^{\mathsf{T}}(\tau)\right)\left(\dot{\mathbf{x}}_l^{\mathsf{T}}(\tau)\ \dot{\mathbf{x}}_r^{\mathsf{T}}(\tau)\right)^{\mathsf{T}} d\tau - \widehat{D}_{pl}\int_0^t \|\dot{\mathbf{x}}_l(\tau)\|^2 d\tau - \frac{\eta}{2}\int_0^t \left\|\dot{\boldsymbol{\xi}}(\tau)\right\|^2 d\tau \tag{54}$$

by [67, Appendix E], where

$$\widehat{D}_{pl} = \eta \min_{i=1,\ldots,N_l}\left\{D_{li} - K_{lci}^2\left(\overline{T}_{li}^2 + \overline{T}_{ri}^2\right)\right\}$$

with $\overline{T}_{li}$ and $\overline{T}_{ri}$ the upper bounds of the communication delays between the local and the remote robots (Assumption A5). By (54), the dynamical controller $\widehat{\Pi}_c$ is passive with respect to the inputs $[\dot{\mathbf{x}}_l\ \dot{\mathbf{x}}_r]$ and the new outputs $[\mathbf{u}_{lc}\ \mathbf{u}_{cr}]$, with the excess of passivity [the last two integral terms in (54)] controlled by the feedforward and feedback loops.

Then, interconnecting the passive dynamical controller $\widehat{\Pi}_c$ with the nonpassive physical component as shown in Fig. 7 can lead to a passive time-delayed teleoperator. Specifically, after adding the time integration of $\dot{\widehat{V}}_p$ in (48) and $\widehat{V}_c$ in (54), the energy stored in the teleoperator,

$$\widehat{V} = (V_3 + V_4) + \left(\widehat{V}_5 + \widehat{V}_6\right) = \widehat{V}_p + \widehat{V}_c \tag{55}$$

can be bounded by

$$\widehat{V}(t) \leq \widehat{V}(0) + \eta\int_0^t \dot{\mathbf{x}}_l^{\mathsf{T}}(\tau)\mathbf{f}_h(\tau)d\tau - \widehat{K}_{pr}\int_0^t \|\mathbf{s}(\tau)\|^2 d\tau - \sum_{i=l,r}\widehat{D}_{pi}\int_0^t \|\dot{\mathbf{x}}_i(\tau)\|^2 d\tau - \widehat{D}_{\xi}\int_0^t \left\|\dot{\boldsymbol{\xi}}(\tau)\right\|^2 d\tau \tag{56}$$

where $\overline{\mathbf{K}}_{pr}(t) \succeq \widehat{K}_{pr}\mathbf{I}_{N_r n}$, $\overline{\mathbf{D}}_{pr} \succeq \widehat{D}_{pr}\mathbf{I}_{N_r n}$, and $\eta\mathbf{I}_{N_l n}/2 - \eta\mathbb{D}_r \succeq \widehat{D}_{\xi}\mathbf{I}_{N_l n}$. The zero sum of the time integrals of the duality product of $[\dot{\mathbf{x}}_l\ \dot{\mathbf{x}}_r]$ and $[\mathbf{u}_{lc}\ \mathbf{u}_{cr}]$ confirms that the physical component of the teleoperator and the dynamical controller $\widehat{\Pi}_c$ in Fig. 7 are interconnected in a power-preserving way. In doing so, the dynamical controller $\widehat{\Pi}_c$ can extract the excess of energy from the physical component through their interconnection, and the feedback loop formed by $\dot{\boldsymbol{\xi}}$ inside $\widehat{\Pi}_c$ can dissipate it to keep the overall teleoperator passive.

The following lemma provides the conditions on the control gains that guarantee the passivity of the teleoperator.

Lemma 4: Consider the bilateral teleoperator with multiple local (1) and remote (2) robots controlled by (38) and (6), respectively. Let the auxiliary variables $\boldsymbol{\xi}_i$ have the dynamics (33) and the sliding variables $\mathbf{s}_i$ be redefined in (34) for all leader remote robots. Under the conditions in Lemma 3, let all D_{li} and D_{ri} be set and all $K_{ri}(t)$ be updated such that $\widehat{D}_{pl}$, $\widehat{D}_{pr}$, $\widehat{K}_{pr}$, and $\widehat{D}_{\xi}$ in (56) are nonnegative.

Then, the teleoperator is passive with respect to the power port $(\mathbf{f}_h, \dot{\mathbf{x}}_l)$. Furthermore, if $\widehat{D}_{pl}$, $\widehat{D}_{pr}$, $\widehat{K}_{pr}$, and $\widehat{D}_{\xi}$ are positive, then $\dot{\mathbf{x}}_l$, $\dot{\mathbf{x}}_r$, $\mathbf{s}$, and $\dot{\boldsymbol{\xi}}$ are square integrable.

In view of (56), the proof of Lemma 4 is straightforward and omitted to save space. From an energy perspective, the feedforward damping at the local robots, $-\mathbf{D}_l\dot{\mathbf{x}}_l$ in $\widehat{\Pi}_c$ in Fig. 7, dissipates both the energy of the physical component and the energy accumulated due to the delay-induced uncertainty $\boldsymbol{\Delta}_{lc}$. The feedback auxiliary dynamics $\dot{\boldsymbol{\xi}}$ split each coupling between a local and a leader remote robot into a series of two springs and dissipate part of the energy of one spring as it transfers the rest to the other spring. The dissipation injected by (40) alleviates the destabilizing effect of $\boldsymbol{\Delta}_{lc}$ in (54) and of $\widehat{\boldsymbol{\Delta}}_r$ in (56). Equation (54) also shows that the dynamics (40) can dissipate and transfer energy only when the energies stored in the two springs are unbalanced, i.e., $\dot{\boldsymbol{\xi}} \neq \mathbf{0}$. Balancing the two springs is not equivalent to depleting them of energy. Therefore, as will be proven in Theorem 1, the synchronization of the local and the remote robots still relies on their damping to deplete them of energy.

Like all damping injection in bilateral teleoperation, the damping in $\mathbf{f}_{li}$ and $\mathbf{f}_{ri}$ can exacerbate the "phantom forces" perceived by the users without correspondence to any remote interaction [69]. Opposing the users' motions, the "phantom forces" increase the users' effort when tele-driving the RMRS, especially for large communication delays. They slow down and tire the users. For smaller delays, lower damping could reduce the "phantom forces" and mitigate the deterioration of performance [70]. Yet, the extra damping injection may cue the users about the velocities of the remote robots through the elastic couplings between them and may contribute to the safe teleoperation of the RMRS by novice users. Future user studies will investigate the impact of damping injection on the bilateral multiuser teleoperation of an RMRS.

C. Steady-State Performance

This section evaluates the steady-state performance of the time-delayed bilateral multiuser teleoperation of an RMRS under the proposed connectivity-preserving passivation control, in two cases: 1) Theorem 1 substantiates the position synchronization and force feedback when passive users manipulate the teleoperator; and 2) Theorem 2 characterizes the spatial distribution of the RMRS based on the locations of the local robots held static by the users.

Theorem 1: Consider the bilateral teleoperator with multiple local (1) and remote (2) robots controlled by (38) and (6), respectively. Define the auxiliary variables $\boldsymbol{\xi}_i$ by (33) and the sliding variables $\mathbf{s}_i$ by (34) for all the leader remote robots. Under the conditions in Lemma 3, let $\widehat{D}_{pl}$, $\widehat{D}_{pr}$, $\widehat{K}_{pr}$, and $\widehat{D}_{\xi}$ in (56) be positive. Then, we have the following.

1) All the local and the remote robots become stationary at infinite time: $\dot{\mathbf{x}}_{li}(t) \to \mathbf{0}$ and $\dot{\mathbf{x}}_{rj}(t) \to \mathbf{0}$ as $t \to +\infty$ for all $i = 1, \ldots, N_l$ and all $j = 1, \ldots, N_r$.
2) The force feedback to each user approaches the sum of all other user forces: $\mathbf{f}_{li}(t) \to \sum_{j\neq i}\mathbf{f}_{hj}(t)$ as $t \to +\infty$ for all $i = 1, \ldots, N_l$.
3) If no users operate their local robots, the positions of all robots converge asymptotically: $\mathbf{x}_{li}(t) - \mathbf{x}_{rj}(t) \to \mathbf{0}$ as $t \to +\infty$ for all $i = 1, \ldots, N_l$ and all $j = 1, \ldots, N_r$.

Proof: The conditions in Lemma 3 guarantee that the tree network of the RMRS is preserved throughout the bilateral teleoperation. Given Assumption A1, positive $\widehat{D}_{pl}$, $\widehat{D}_{pr}$, $\widehat{K}_{pr}$, and $\widehat{D}_{\xi}$ lead to $\{\dot{\mathbf{x}}_l, \dot{\mathbf{x}}_r, \mathbf{s}, \dot{\boldsymbol{\xi}}\} \in \mathcal{L}_2$ by Lemma 4. Furthermore, (46), (53), (55), and (56) together indicate that V_3, V_4, $\widehat{V}_5$, and $\widehat{V}_6$ are upper-bounded. By (13) and (23), finite V_3 in (15) ensures finite

$[\mathbf{L}(\mathbf{x}_r)\otimes\mathbf{I}_n]\mathbf{x}_r$ and $\mathbf{s}$. Similarly, $\dot{\mathbf{x}}_l$ is finite because V_4 in (25) is upper-bounded. Finite $\widehat{V}_5$ in (49) and $\widehat{V}_6$ in (51) guarantee that $\mathbb{I}\mathbf{x}_r-\boldsymbol{\xi}$ and $\mathbf{x}_l-\boldsymbol{\xi}$ are bounded, respectively. Then, using (36) and (40), it follows that $\{\dot{\mathbf{x}}_l,\dot{\mathbf{x}}_r,\mathbf{s},\dot{\boldsymbol{\xi}}\}\in\mathcal{L}_\infty\cap\mathcal{L}_2$ and thus that $\{\dot{\mathbf{x}}_l(t),\dot{\mathbf{x}}_r(t),\mathbf{s}(t),\dot{\boldsymbol{\xi}}(t)\}\to\mathbf{0}$ as $t\to+\infty$.

Given Assumptions A2 and A5, the time derivative of (39) leads to bounded $\ddot{\mathbf{x}}_l$. Then, by Barbalat's lemma, $\dot{\mathbf{x}}_l(t)\to\mathbf{0}$ implies that $\ddot{\mathbf{x}}_l(t)\to\mathbf{0}$. Furthermore, $\dot{\mathbf{x}}_l(t)\to\mathbf{0}$ and $\dot{\boldsymbol{\xi}}(t)\to\mathbf{0}$ make $\mathbf{u}_{lc}(t)\to-\mathbf{u}_{lcd}(t)\to\mathbf{u}_{ldc}(t)$. Then, (39) and (40) lead to $\mathbf{u}_{lc}(t)+\mathbb{I}\mathbf{u}_{cr}(t)\to\mathbf{0}$ as $t\to+\infty$. From $(\mathbf{1}_{N_r}\otimes\mathbf{I}_n)^{\mathsf{T}}\mathbf{u}_{cr}=[(\mathbf{1}_{N_l}^{\mathsf{T}}\,\mathbf{1}_{N_r-N_l}^{\mathsf{T}})\otimes\mathbf{I}_n]\mathbf{u}_{cr}=[(\mathbf{1}_{N_l}^{\mathsf{T}}\,\mathbf{0}_{N_r-N_l}^{\mathsf{T}})\otimes\mathbf{I}_n]\mathbf{u}_{cr}=(\mathbf{1}_{N_l}\otimes\mathbf{I}_n)^{\mathsf{T}}\mathbb{I}\mathbf{u}_{cr}$, it follows that

$$\lim_{t\to+\infty}\eta\left(\mathbf{1}_{N_r}\otimes\mathbf{I}_n\right)^{\mathsf{T}}\mathbf{u}_{cr}(t)+\eta\left(\mathbf{1}_{N_l}\otimes\mathbf{I}_n\right)^{\mathsf{T}}\mathbf{u}_{lc}(t)$$
$$=\lim_{t\to+\infty}\eta\left(\mathbf{1}_{N_l}\otimes\mathbf{I}_n\right)^{\mathsf{T}}[\mathbb{I}\mathbf{u}_{cr}(t)+\mathbf{u}_{lc}(t)]=\mathbf{0}. \tag{57}$$

Furthermore, $\dot{\mathbf{x}}_r(t)\to\mathbf{0}$, $\mathbf{s}(t)\to\mathbf{0}$, and (36) imply that $\eta\mathbf{u}_{cr}(t)\to-\sigma[\mathbf{L}(\mathbf{x}_r(t))\otimes\mathbf{I}_n]\mathbf{x}_r(t)$. From $\eta\sum_{i=1}^{N_l}\mathbf{f}_{li}=\sigma[\mathbf{1}_{N_r}^{\mathsf{T}}\mathbf{L}(\mathbf{x}_r)\otimes\mathbf{I}_n]\mathbf{x}_r-\eta(\mathbf{1}_{N_l}\otimes\mathbf{I}_n)^{\mathsf{T}}\mathbf{u}_{lc}=\sigma(\mathbf{1}_{N_r}\otimes\mathbf{I}_n)^{\mathsf{T}}[\mathbf{L}(\mathbf{x}_r)\otimes\mathbf{I}_n]\mathbf{x}_r-\eta(\mathbf{1}_{N_l}\otimes\mathbf{I}_n)^{\mathsf{T}}\mathbf{u}_{lc}$, it follows that

$$\lim_{t\to+\infty}\eta\left(\mathbf{1}_{N_r}\otimes\mathbf{I}_n\right)^{\mathsf{T}}\mathbf{u}_{cr}(t)+\eta\left(\mathbf{1}_{N_l}\otimes\mathbf{I}_n\right)^{\mathsf{T}}\mathbf{u}_{lc}(t)$$
$$=-\lim_{t\to+\infty}\sigma\left(\mathbf{1}_{N_r}\otimes\mathbf{I}_n\right)^{\mathsf{T}}\left[\mathbf{L}(\mathbf{x}_r(t))\otimes\mathbf{I}_n\right]\mathbf{x}_r(t)$$
$$+\lim_{t\to+\infty}\eta\left(\mathbf{1}_{N_l}\otimes\mathbf{I}_n\right)^{\mathsf{T}}\mathbf{u}_{lc}(t)=-\lim_{t\to+\infty}\eta\sum_{i=1}^{N_l}\mathbf{f}_{li}(t). \tag{58}$$

Together, (57) and (58) lead to $\lim_{t\to+\infty}\sum_{i=1}^{N_l}\mathbf{f}_{li}(t)=\mathbf{0}$. From $\dot{\mathbf{x}}_{li}(t)\to\mathbf{0}$, $\ddot{\mathbf{x}}_{li}(0)\to\mathbf{0}$, and the dynamics (1) of the local robots, it follows that $-\mathbf{f}_{li}(t)\to\mathbf{f}_{hi}(t)$ as $t\to+\infty$ for all $i=1,\ldots,N_l$. Thus, force feedback is achieved in the steady state, $\mathbf{f}_{li}(t)\to\sum_{j\neq i}\mathbf{f}_{hj}(t)$ as $t\to+\infty$.

When no users operate their local robots, namely, $\mathbf{f}_{hi}=\mathbf{0}$ for all $i=1,\ldots,N_l$, then $\dot{\mathbf{x}}_l(t)\to\mathbf{0}$ and $\ddot{\mathbf{x}}_l\to\mathbf{0}$ and (39) imply that $\mathbf{u}_{lcd}(t)\to\mathbf{0}$. Also, $\dot{\boldsymbol{\xi}}(t)\to\mathbf{0}$ and (40) lead to $\mathbf{u}_{ldc}(t)+\mathbb{I}\mathbf{u}_{cr}(t)\to\mathbf{0}$ as $t\to+\infty$. Together, $\dot{\mathbf{x}}_l(t)\to\mathbf{0}$ and $\dot{\boldsymbol{\xi}}(t)\to\mathbf{0}$ yield $\mathbf{x}_l(t)\to\boldsymbol{\xi}(t)\to\mathbb{I}\mathbf{x}_r(t)$. Then, $\mathbf{u}_{cr}$ in (36) implies that $\mathbf{u}_{cr}(t)\to\mathbf{0}$ and thus that $[\mathbf{L}(\mathbf{x}_r(t))\otimes\mathbf{I}_n]\mathbf{x}_r(t)\to\mathbf{0}$ by $\dot{\mathbf{x}}_r(t)\to\mathbf{0}$ and $\mathbf{s}(t)\to\mathbf{0}$. The preserved tree network of the RMRS then ensures the convergence of the positions of the remote robots: $\mathbf{x}_{ri}(t)-\mathbf{x}_{rj}(t)\to\mathbf{0}$ for all $i,j=1,\ldots,N_r$. Together with $\mathbf{x}_l(t)\to\mathbb{I}\mathbf{x}_r(t)$, it implies the synchronization of all robots: $\mathbf{x}_{li}(t)-\mathbf{x}_{rj}(t)\to\mathbf{0}$ as $t\to+\infty,\forall i=1,\ldots,N_l$ and $\forall j=1,\ldots,N_r$. ■

Theorem 1 shows that, during the steady state, the proposed multiuser teleoperation of a freely moving RMRS with undirected communications applies to each user the sum of the forces of all other users. Hence, it enables all users to feel their peers' intentions in applications like the cooperative teledeployment of a robotic sensor network. During the transient phase, the couplings between the local and the remote robots may also convey to the users the dynamics of their associated leader remote robots.

The bilateral multiuser teleoperation of an RMRS in physical interaction with the environment remains an open problem. For the single-user teleoperation of an RMRS with undirected communications, a passivity-constrained optimization [19] dynamically scales the viscoelastic couplings between the leader remote robot and its neighbors, but requires the leader remote robot to estimate the interactions with the environment of all the remote robots and to broadcast optimal scaling factors to all its neighbors. For the multiuser teleoperation of an RMRS with directed communications, the lack of directed transmission paths between any pair of the leader remote robots may thwart the transfer of some user forces to the other users. Nevertheless, future work will explore extensions of the proposed control that can convey to the users the interactions of the remote robots with the environment in a distributed fashion and over a directed communication network.

While Theorem 1 investigates the position synchronization and force feedback performance of the multiuser multirobot teleoperation system in the steady state, Theorem 2 resolves the spatial distribution of the RMRS in the steady state.

Theorem 2: Consider the bilateral teleoperator with multiple local (1) and remote (2) robots controlled as in Theorem 1. Let all users hold their local robots immobile, i.e., $\dot{\mathbf{x}}_{li}(t)=\mathbf{0}$ and $\mathbf{x}_{li}(t)=\mathbf{x}_{li}^*$ for all $i=1,\ldots,N_l$ and all $t\geq0$. Then, all the remote robots converge asymptotically to the convex hull spanned by all the local robots, namely, $\dot{\mathbf{x}}_{ri}(t)\to\mathbf{0}$ and $\mathbf{x}_{ri}(t)\to\mathbf{x}_{ri}^*\in\mathcal{C}_h$ with

$$\mathcal{C}_h=\left\{\sum_{j=1}^{N_l}\lambda_j\mathbf{x}_{lj}^*\,\middle|\,\lambda_j\geq0\text{ and }\sum_{j=1}^{N_l}\lambda_j=1\right\}.$$

Proof: When all users hold their local robots fixed, $\dot{\mathbf{x}}_l(t)=\mathbf{0}$ for all $t\geq0$, they inject no energy into the teleoperator, which itself is passive with the proposed controller. Theorem 1 then leads to $\{\dot{\mathbf{x}}_r,\mathbf{s},\dot{\boldsymbol{\xi}}\}\in\mathcal{L}_\infty\cap\mathcal{L}_2$, and further to $\dot{\mathbf{x}}_r(t)\to\mathbf{0}$, $\mathbf{s}(t)\to\mathbf{0}$, and $\dot{\boldsymbol{\xi}}(t)\to\mathbf{0}$ as $t\to+\infty$.

Define $\widehat{\mathbf{K}}(t)=\mathrm{Diag}\{\widehat{\mathbf{K}}_{cri}(t)\}$ with $\widehat{\mathbf{K}}_{cri}(t)$ given by $\widehat{\mathbf{K}}_{cri}(t)(\mathbf{x}_{ri}-\boldsymbol{\xi}_i)=\overline{\mathbf{F}}_{hi}\cdot\tanh[K_{cri}(\mathbf{x}_{ri}-\boldsymbol{\xi}_i)]$ for $i=1,\ldots,N_l$. Note that $\widehat{\mathbf{K}}(t)$ is diagonal and uniformly positive definite, namely, $\widehat{\mathbf{K}}(t)\succ\epsilon\mathbf{I}_{N_ln}$ for some $\epsilon>0$ as $\mathbf{x}_{ri}-\boldsymbol{\xi}_i$ are bounded. Let $\mathbb{L}(t)=\mathbf{L}(\mathbf{x}_r(t))\otimes\mathbf{I}_n$. Then, $\mathbf{u}_{cr}$ becomes $\mathbf{u}_{cr}=\mathbb{I}^{\mathsf{T}}\widehat{\mathbf{K}}(t)(\mathbb{I}\mathbf{x}_r-\boldsymbol{\xi})$; the steady-state dynamics (36) of $\widehat{\Pi}_1$ become

$$\lim_{t\to+\infty}\dot{\mathbf{x}}_r(t)=-\lim_{t\to+\infty}\left[\eta\mathbb{I}^{\mathsf{T}}\widehat{\mathbf{K}}(t)\mathbb{I}+\sigma\mathbb{L}(t)\right]\mathbf{x}_r(t)$$
$$+\lim_{t\to+\infty}\eta\mathbb{I}^{\mathsf{T}}\widehat{\mathbf{K}}(t)\boldsymbol{\xi}(t)=\mathbf{0}$$

and the steady-state dynamics (40) of $\boldsymbol{\xi}$ become

$$\lim_{t\to+\infty}\dot{\boldsymbol{\xi}}(t)=-\lim_{t\to+\infty}\left[\mathbf{K}_{lc}+\mathbb{I}\mathbb{I}^{\mathsf{T}}\widehat{\mathbf{K}}(t)\right]\boldsymbol{\xi}(t)$$
$$+\lim_{t\to+\infty}\mathbb{I}\mathbb{I}^{\mathsf{T}}\widehat{\mathbf{K}}(t)\mathbb{I}\mathbf{x}_r(t)+\mathbf{K}_{lc}\mathbf{x}_l^*=\mathbf{0}.$$

Using $\mathbb{I}\mathbb{I}^{\mathsf{T}}=\mathbf{I}_{N_ln}$, the two steady-state dynamics $\dot{\mathbf{x}}_r$ and $\dot{\boldsymbol{\xi}}$ can be rewritten as

$$-\lim_{t\to+\infty}\widehat{\mathbf{L}}(t)\begin{bmatrix}\boldsymbol{\xi}(t)\\\frac{1}{\sqrt{\eta}}\mathbf{x}_r(t)\end{bmatrix}+\begin{bmatrix}\mathbf{K}_{lc}\mathbf{x}_l^*\\\mathbf{0}\end{bmatrix}=\begin{bmatrix}\mathbf{0}\\\mathbf{0}\end{bmatrix} \tag{59}$$

where $\widehat{\mathbf{L}}(t)$ is given by

$$\widehat{\mathbf{L}}(t) = \begin{bmatrix} \mathbf{I}_{N_l n} \\ -\sqrt{\eta}\mathbb{I}^{\mathsf{T}} \end{bmatrix} \widehat{\mathbf{K}}(t) \begin{bmatrix} \mathbf{I}_{N_l n} & -\sqrt{\eta}\mathbb{I} \end{bmatrix} + \begin{bmatrix} \mathbf{K}_{lc} & \mathbf{0} \\ \mathbf{0} & \sigma\mathbb{L}(t) \end{bmatrix}$$

and is clearly uniformly positive semidefinite.

The proof that $\widehat{\mathbf{L}}(t) \succ \mathbf{0}$ is by contradiction. Suppose that $\widehat{\mathbf{L}}(t)$ has a nontrivial null space. Then, there exists a nonzero vector $\mathbf{v} = (\mathbf{v}_1^{\mathsf{T}} \ \mathbf{v}_2^{\mathsf{T}})^{\mathsf{T}}$ such that $\mathbf{v}^{\mathsf{T}}\widehat{\mathbf{L}}(t)\mathbf{v} = (\mathbf{v}_1^{\mathsf{T}} - \sqrt{\eta}\mathbf{v}_2^{\mathsf{T}}\mathbb{I}^{\mathsf{T}})\widehat{\mathbf{K}}(t)(\mathbf{v}_1 - \sqrt{\eta}\mathbb{I}\mathbf{v}_2) + \mathbf{v}_1^{\mathsf{T}}\mathbf{K}_{lc}\mathbf{v}_1 + \sigma\mathbf{v}_2^{\mathsf{T}}\mathbb{L}(t)\mathbf{v}_2 = 0$. Because $\mathbf{K}_{lc} \succ \mathbf{0}$, $\widehat{\mathbf{K}}(t) \succ \mathbf{0}$, and $\mathbb{L}(t)$ is a weighted Laplacian matrix, $\mathbf{v}^{\mathsf{T}}\widehat{\mathbf{L}}(t)\mathbf{v} = 0$ requires that $\mathbf{v}_1 = \mathbf{0}$, $\mathbf{v}_2 = \mu\mathbf{1}_{N_r n}$ and $\mathbf{v}_1 = \sqrt{\eta}\mathbb{I}\mathbf{v}_2$ for some integer μ. By the definition of $\mathbb{I}$, this is possible only if $\mu = 0$ and thus $\mathbf{v} = \mathbf{0}$, which contradicts the hypothesis that $\widehat{\mathbf{L}}(t)$ has a nontrivial null space.

Being a nonsingular M-matrix, $\widehat{\mathbf{L}}(t)$ has, thus, a nonnegative inverse $\widehat{\mathbf{L}}^{-1}(t)$. It then follows that

$$\mathbf{H}(t) = \begin{bmatrix} \mathbf{I}_{N_l n} & \mathbf{0} \\ \mathbf{0} & \sqrt{\eta}\mathbf{I}_{N_r n} \end{bmatrix} \widehat{\mathbf{L}}^{-1}(t) \begin{bmatrix} \mathbf{K}_{lc} \\ \mathbf{0} \end{bmatrix}$$

is also nonnegative. Nevertheless, $\mathbf{H}(t)$ depends on the states of the teleoperator because $\mathbb{L}(t)$ and $\widehat{\mathbf{K}}(t)$ in $\widehat{\mathbf{L}}(t)$ are state-dependent. The spatial distribution of all the remote robots can be derived by post- and premultiplying $\widehat{\mathbf{L}}(t)$ as follows:

$$\mathbf{1} = \begin{bmatrix} \mathbf{I}_{N_l n} & \mathbf{0} \\ \mathbf{0} & \sqrt{\eta}\mathbf{I}_{N_r n} \end{bmatrix} \widehat{\mathbf{L}}^{-1}(t)\widehat{\mathbf{L}}(t) \begin{bmatrix} \mathbf{1}_{N_l n} \\ \frac{1}{\sqrt{\eta}}\mathbf{1}_{N_r n} \end{bmatrix} = \mathbf{H}(t)\mathbf{1}_{N_l n}$$

which implies that every row of $\mathbf{H}(t)$ sums to 1. As a result, the steady-state locations of all the remote robots can be derived by solving (59) by

$$\begin{aligned} &- \lim_{t\to+\infty} \begin{bmatrix} \mathbf{I}_{N_l n} & \mathbf{0} \\ \mathbf{0} & \sqrt{\eta}\mathbf{I}_{N_r n} \end{bmatrix} \widehat{\mathbf{L}}^{-1}(t)\widehat{\mathbf{L}}(t) \begin{bmatrix} \boldsymbol{\xi}(t) \\ \frac{1}{\sqrt{\eta}}\mathbf{x}_r(t) \end{bmatrix} \\ &+ \lim_{t\to+\infty} \begin{bmatrix} \mathbf{I}_{N_l n} & \mathbf{0} \\ \mathbf{0} & \sqrt{\eta}\mathbf{I}_{N_r n} \end{bmatrix} \widehat{\mathbf{L}}^{-1}(t) \begin{bmatrix} \mathbf{K}_{lc}\mathbf{x}_l^* \\ \mathbf{0} \end{bmatrix} \\ &= - \lim_{t\to+\infty} \begin{bmatrix} \boldsymbol{\xi}(t) \\ \mathbf{x}_r(t) \end{bmatrix} + \lim_{t\to+\infty} \mathbf{H}(t)\mathbf{x}_l^* = \begin{bmatrix} \mathbf{0} \\ \mathbf{0} \end{bmatrix}. \end{aligned}$$

Although $\mathbf{H}(t)$ is state-dependent, the sum of each of its rows is invariably 1. Thus, all the remote robots approach the convex hull $\mathcal{C}_h$ formed by all the local robots asymptotically. A more detailed proof is presented in [67]. ■

Compared to the containment control of autonomous multirobot systems, Theorem 2 formulates the problem in the context of bilateral multiuser teleoperation of an RMRS. The containment control through bilateral teleoperation can be advantageous because it permits the dynamic redeployment of an RMRS based on the physical interactions among multiple users. For example, in spatiotemporal sampling, the assignment of a robotic sensor network could be determined interactively through haptic negotiations among its human operators instead of being fixed or preprogrammed. The connectivity and passivity analyses in Sections IV-A and IV-B guarantee the safety of the physical interaction with the robotic system. Furthermore, the force feedback and position synchronization, guaranteed in Theorem 1, enable all users to perceive the intentions of the other users and to impose their decisions on the RMRS. Finally, Theorem 2 clarifies the active role that the human operators play in altering the spatial layout of the RMRS.

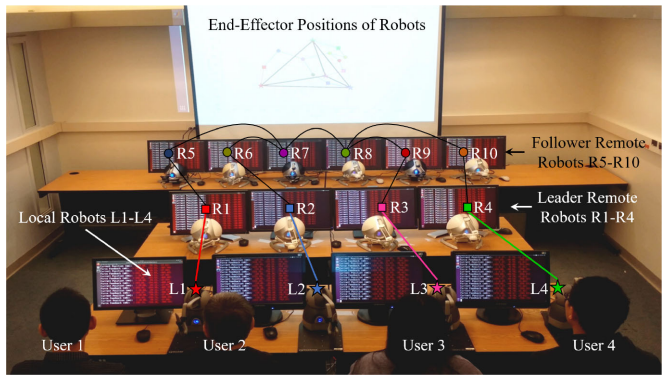

Fig. 8. Snapshot from the experiments. The colored lines are the time-delayed communications between the local and the remote robots. The black lines are the proximity-limited communications between the remote robots.

V. Experimental Results

This section compares the proposed connectivity-preserving passivation strategy to P+d control through two experiments on a teleoperation platform with four local and ten remote robots. The experimental results substantiate that both controls can stabilize the time-delayed multiuser teleoperation of an RMRS. However, P+d control may fail to preserve the connectivity of the RMRS and, thus, to support the multiuser collaboration when deploying the remote robots. In contrast, the strategy proposed in this article maintains all communication links of the tree network of the RMRS regardless of how fast the users change their commands. Thus, it enables all users to participate in the containment control of the RMRS. A video of the experiments can be found online.[1]

As shown in Fig. 8, the experimental platform comprises four Geomagic Touch[2] local robots (L1-L4) and an RMRS with ten Novint Falcon[3] remote robots (R1–R10). Each robot is controlled locally via USB 2.0 by a C++ program running on a unique dedicated Ubuntu machine at 1 kHz. The C++ programs can obtain position measurements of, and impose control forces on, the robot end-effectors in their local East, North, Up Cartesian coordinate systems by calling the standard haptic APIs: the OpenHaptics toolkit for the local robots and the CHAI3D[4] SDK for the remote robots. The programs can further compute the velocities of the robot end-effectors from the position measurements using second-order low-pass filters with a cutoff frequency of 100 Hz. All machines connect to a 16-port network switch, the NETGEAR GS316, and further to the Internet through Insignia CAT-6 ethernet cables. They run the Robot Operating System (ROS) to send/read position signals

[1][Online]. Available: https://youtu.be/ZPoNZW-dYkw
[2][Online]. Available: https://www.3dsystems.com/haptics-devices/touch
[3][Online]. Available: https://en.wikipedia.org/wiki/Novint_Technologies
[4][Online]. Available: https://www.chai3d.org

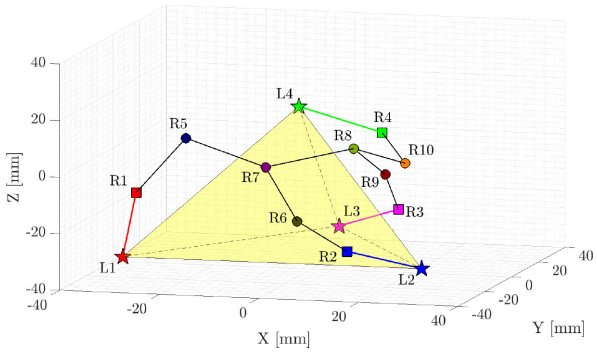

Fig. 9. Initial positions of the robots and their communication links. The yellow tetrahedron is the convex hull formed by the local robots. The communication range of the remote robots is $r = 30$ mm.

to/from other robots at an approximate rate of 50 Hz. The local control loops of all robots run at a higher frequency (1 kHz) than the ROS interface (50 Hz), and thus, the robot positions are delayed by up to 40 ms when received by, and employed in the control of, their neighbors.

Controlling the local Geomagic Touch and remote Novint Falcon robots is challenging because they all are haptic devices with limited performance. The inexact gravity compensation and the inherent dry friction of the robots severely limit their motion accuracy. Moreover, damping injection through control can lead to instability because of velocity estimation errors. The experiments address these practical challenges by abstracting all the local robots by point proxies with mass 10 g and all the remote robots by point proxies with mass 100 g, coupling all the local robots to their proxies for bilateral teleoperation, controlling the remote robots to track their proxies, and tuning the control gains that connect the robots to their proxies so as to permit to assume that the proxies adequately represent the dynamics of the physical robots and to carry out the experimental comparison in the virtual (proxy) layer. Additionally, the positions of the virtual proxies are projected on a screen (see Fig. 8).

As illustrated in Section IV, the proposed control inherits the position synchronization and force feedback capabilities of P+d control and also preserves the proximity-constrained communications between the remote robots. The experiments validate the results in Section IV using the following seven steps.

A. *Autonomous Mode*

1) Regulate all the local (L1–L4) and the remote (R1–R10) robots to their initial positions depicted in Fig. 9.
2) Activate the controllers of the remote robots and keep the local robots at their initial positions.
3) Activate the controllers of the local robots without applying any user forces to the robots.

T. *Teleoperation Mode*

4) User 1 repetitively strains and relaxes the coupling between the local robot L1 and the remote robot R1.
5) All users cooperatively change the spatial distribution of the RMRS.
6) User 1 yanks and releases their local robot L1 regardless of the connectivity of the RMRS.

TABLE I
AGGRESSIVENESS Ξ OF THE ACTIONS OF USER 1 DURING STEP 6 OF THE TELEOPERATION

	Aggressiveness Metric Ξ				
P+d Control	0.11	0.14	0.17	0.10	0.16
	0.61	1.78	0.13	0.13	1.75
The Proposed Design	0.11	0.11	0.39	0.11	0.17
	0.18	1.79	1.85	1.83	1.89
	0.14	0.23	0.58	0.24	0.33
	1.91	1.93	2.26	1.95	0.12
	0.15	0.16			

7) All users move their local robots close to their original positions.

In the autonomous mode, Step 1 initializes the states (positions and velocities) of all robots to guarantee Assumptions A3 and A4, Step 2 evaluates the containment control in Theorem 2, and Step 3 investigates the autonomous synchronization of all robots in Theorem 1. In the subsequent teleoperation mode, the four operators use their local robots to teleoperate the RMRS: Step 4 tests the steady-state force feedback in Theorem 1, Step 5 verifies that the robust synchronization in Theorem 1 enables the users to collectively tele-guide the RMRS, Step 6 compares connectivity preservation for the RMRS under the proposed and under P+d control, and Step 7 demonstrates the need to preserve the connectivity of the RMRS during teleoperation.

In the comparison in Step 6, users 2–4 keep their local robots L2–L4 in a fixed triangle at the top right corner of the workspace, while user 1 repeatedly yanks their local robot L1 from near the fixed triangle to the bottom left corner of the workspace, to endanger the connectivity of the RMRS. The average acceleration of L1, $\Xi = 4\,d/t^2$ with d its travel distance and t its travel time, provides an empiric aggressiveness metric for the user's motions. Table I lists the aggressiveness Ξ of all user trials in Step 6 for both experiments chronologically, from left to right and from up to down. The mean values of the aggressiveness metric Ξ for the ten trials in the first experiment and for the 22 trials in the second experiment are $\overline{\Xi}_1 = 0.51$ and $\overline{\Xi}_2 = 0.84$, with standard deviations $\sigma_1 = 0.68$ and $\sigma_2 = 0.85$, respectively. Thus, user 1 poses a greater threat to the connectivity of the RMRS in the second experiment. Nevertheless, the experimental results in Sections V-A and V-B will demonstrate that the proposed control, unlike P+d control, preserves all initial couplings between the remote robots.

Due to their limited workspaces, the communication radius is set to $r = 30$ mm for all the remote Novint Falcon robots (see Fig. 9). In addition to the masses of the virtual proxies, the injected damping impacts the quality of the user experience during teleoperation. On the one hand, sufficient damping stabilizes the system and suppresses unwanted robot vibrations. On the other hand, too much damping demands increased user effort and tires the operator. For both experiments, the damping gains $D_* = 1$ for all robots are first selected heuristically, to support high-quality user experience. Then, the proportional control gains $P_* = 1500$ are tuned for tight but stable synchronization of all robots. Trial and error indicates that P+d control cannot maintain the RMRS connected when user 1 applies forces larger than 3 N as the other users keep their local robots stationary.

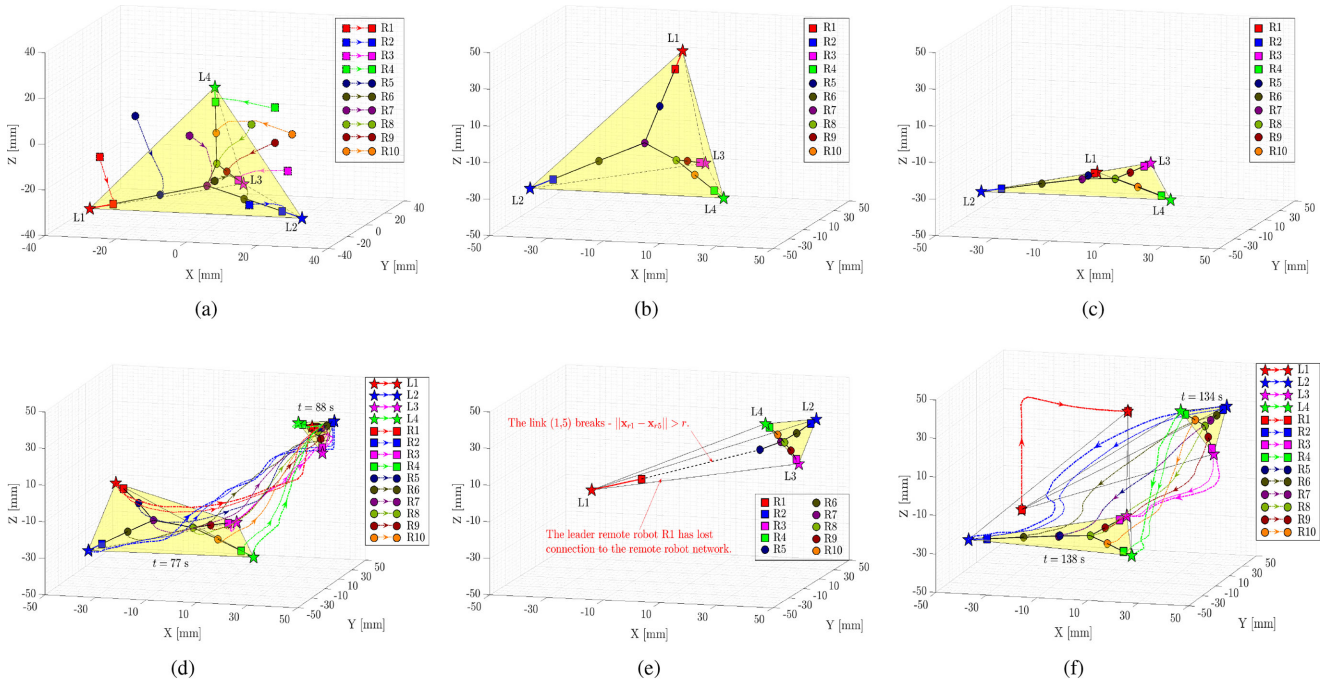

Fig. 10. Experimental four-user teleoperation of a ten-robot RMRS under P+d control: the robot positions/paths and their network interconnections at/during some time instants/periods of the experiment. In (a)–(d), the RMRS is connected and all users impact its spatial distribution. In (e), a motion of user 1 with $\Xi = 1.78$ destroys the communication link between the remote robots R1 and R5. Thereafter, user 1 cannot tele-guide the RMRS [see (f)]. (a) Step 2, from $t = 35$ s to $t = 42$ s. (b) Step 4, at $t = 58$ s. (c) Step 4, at $t = 60$ s. (d) Step 5, from $t = 77$ s to $t = 88$ s. (e) Step 6, at $t = 107$ s. (f) Step 7, from $t = 134$ s to $t = 138$ s.

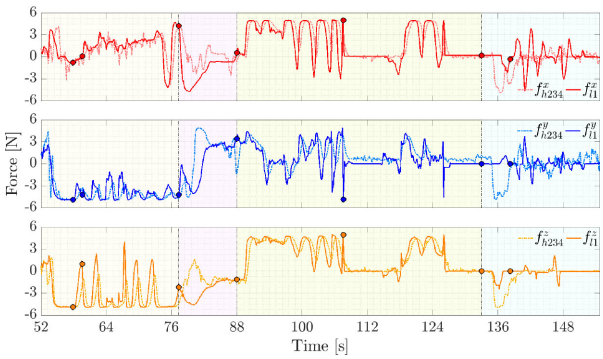

Fig. 11. Control force $\mathbf{f}_{l1} = (f^x_{l1}, f^y_{l1}, f^z_{l1})^\mathsf{T}$ of the local robot L1 and the sum $\mathbf{f}_{h234} = (f^x_{h234}, f^y_{h234}, f^z_{h234})^\mathsf{T}$ of the forces of users 2–4, during the experimental teleoperation under P+d control.

Therefore, the couplings between the local robots and their proxies, and between the proxies of the local and the leader remote robots, are saturated by $\overline{\mathbf{f}}_{hi} = (5, 5, 5)^\mathsf{T}$ N. Finally, the gains of the proposed control are chosen $P = 1$, $Q = 0.01$, $\sigma = 50$, $\eta = 1$, and $K_* = 1000$ for connectivity-preserving teleoperation.

The remainder of this section contrasts the connectivity-preserving synchronization performance of P+d control to that of the proposed design in Figs. 10 and 12. Figs. 11 and 13 depict the control force $\mathbf{f}_{l1}$ of the local robot L1 and the sum $\mathbf{f}_{h234} = \mathbf{f}_{h2} + \mathbf{f}_{h3} + \mathbf{f}_{h4}$ of the forces applied by users 2–4, to illustrate the force feedback performance. Because the robots lack force measurement, all the user forces $\mathbf{f}_{hi}$ are approximated by the coupling forces between the local robots and their proxies.

A. *Teleoperation With P+d Control*

Fig. 10 presents the experimental four-user teleoperation of a ten-robot RMRS under P+d control during various steps of the experimental procedure. Fig. 10(a) plots the paths of the remote robots (R1–R10) in Step 2, from their initial positions (markers with dashed edges) at $t = 35$ s to their final positions (markers with solid edges) inside the convex hull spanned by all the local robots (L1–L4) at $t = 42$ s. It illustrates that P+d control is a suitable containment strategy given a connected RMRS. Fig. 10(b) and (c) depicts all robot positions at two time instants when user 1 strains at $t = 58$ s and then restores at $t = 60$ s, the coupling between their local robot L1 and the leader remote robot R1 in Step 4. They confirm that the RMRS behaves as an elastic body that deforms as a result of its interactions with the four users. Fig. 10(d) shows the paths of the robots from $t = 77$ s to $t = 88$ s in Step 5, when the four users move their local robots to carry the connected RMRS to another area. The arrows on the paths indicate the movement directions. Once the RMRS has reached the new area, user 1 recommences to strain the coupling between the robots L1 and R1, this time with larger and faster motions. Fig. 10(e) shows that a sudden motion of user 1, with $\Xi = 1.78$, accelerates the remote robot R1 so much that its neighbor R5 cannot follow it sufficiently fast. As a result, at $t = 107$ s in Step 6, their interdistance grows larger than their communication range r and their communication link breaks [the dashed line in Fig. 10(e)], disconnecting R1 from the rest of the RMRS. Fig. 10(f) displays the retraction of all local robots close to their original positions from $t = 134$ s to $t = 138$ s in Step 7. Note that, because the remote robot R1 is

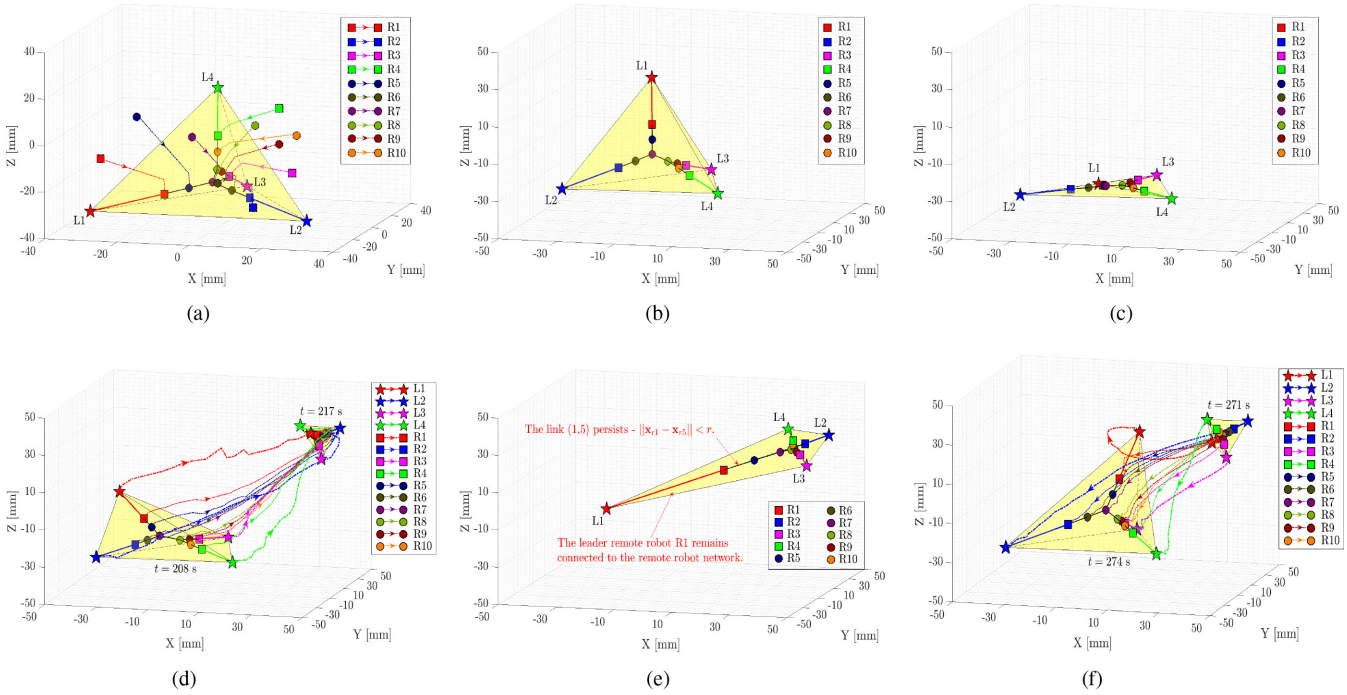

Fig. 12. Experimental four-user teleoperation of a ten-robot RMRS under the proposed connectivity-preserving feedforward–feedback passivation control. (a)–(d) validate the containment control of the RMRS and its cooperative transportation by all users. Most importantly, (e) shows that the proposed controller can preserve all communication links between the remote robots even when the users steer it aggressively with $\Xi > 1.78$ and thus permits all users to contribute to the deployment of the RMRS throughout the teleoperation [see (f)]. (a) Step 2, from $t = 158$ s to $t = 167$ s. (b) Step 4, at $t = 195$ s. (c) Step 4, at $t = 196$ s. (d) Step 5, from $t = 208$ s to $t = 217$ s. (e) Step 6, at $t = 255$ s. (f) Step 7, from $t = 271$ s to $t = 274$ s.

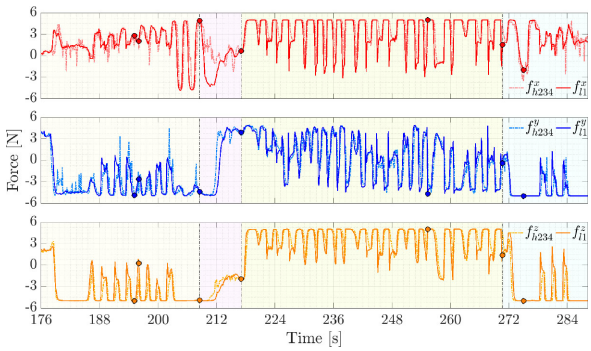

Fig. 13. Control force $\mathbf{f}_{l1} = (f^x_{l1}, f^y_{l1}, f^z_{l1})^\mathsf{T}$ of the local robot L1 and the sum $\mathbf{f}_{h234} = (f^x_{h234}, f^y_{234}, f^z_{h234})^\mathsf{T}$ of the forces of users 2–4, during the experimental teleoperation under the proposed connectivity-preserving feedforward–feedback passivation control.

disconnected from all the other remote robots in this step, user 1 controls only the motion of R1. In practice, it may be undesirable that any user loses their ability to tele-guide the RMRS.

In Step 6, user 1 yanks their local robot L1 ten times, from $t = 89$ s to $t = 130$ s in the accompanying video, to examine the connectivity of the RMRS under P+d control. Table I lists the aggressiveness Ξ of all the motions of user 1, in chronological order, from left to right and from up to down. The experimental results show that the RMRS remains connected for the motions of user 1 with $\Xi \leq 0.61$, and it disconnects for Ξ increasing to 1.75 and 1.78 [see Fig. 10(e)].

Fig. 11 plots the force feedback $\mathbf{f}_{l1} = (f^x_{l1}, f^y_{l1}, f^z_{l1})^\mathsf{T}$ to user 1 and the sum $\mathbf{f}_{h234} = (f^x_{h234}, f^y_{h234}, f^z_{h234})^\mathsf{T}$ of all other user-applied forces. In the plots, the areas colored in light yellow, pink, green, and blue indicate Steps 4–7 in the teleoperation mode, and the seven dots indicate the forces that correspond to the states of the system at $t = 58$ s, $t = 60$ s, $t = 77$ s, $t = 88$ s, $t = 107$ s, $t = 134$ s, and $t = 138$ s in Fig. 10. As the local robot L1 moves to its position in Fig. 10(b) guided by its user and then moves to its position in Fig. 10(c) when released by its user, the force feedback f^z_{l1} approaches -5 N and then drops to near 0 N in the yellow area in Fig. 11. In Step 5, all users cooperatively move the RMRS as shown in Fig. 10(d) and reduce the volume of the tetrahedron spanned by their local robots. Hence, the force feedback $\mathbf{f}_{l1}$ to user 1 becomes approximately zero in the pink area in Fig. 11. Then, user 1 yanks their local robot L1 and f^x_{l1} and f^z_{l1} reach their upper bound 5 N repeatedly in the green area of Fig. 11, until the communication link (1, 5) breaks the seventh time [see Fig. 10(e)]. While the link (1, 5) is broken, the robots L1 and R1 are synchronized and detached from the other robots, and the force feedback $\mathbf{f}_{l1}$ becomes $\mathbf{0}$. Later, user 1 reconnects the robots R1 and R5 and yanks L1 repeatedly again, breaking the link (1, 5) the third time. When all users slowly move their local robots close to their initial locations in Fig. 10(f), the detached L1–R1 robot pair conveys almost no force feedback to user 1. From $t = 138$ s to $t = 150$ s, user 1 wiggles L1 quickly to make R1 lag far behind L1 and feels stronger force feedback due to the dynamics of R1. Fig. 11 shows that P+d control can display to user 1 the sum of all other

user forces when the RMRS is connected, especially when the coupling between L1 and R1 is stretched. When the link (1, 5) is broken and the RMRS is disconnected, the force feedback $\mathbf{f}_{l1}$ no longer conveys $\mathbf{f}_{h234}$, see their large discrepancy after $t = 139$ s in Fig. 11.

In summary, P+d control stabilizes the bilateral teleoperation, achieves containment control of a connected RMRS, and conveys the sum of all other user forces to each operator, but cannot preserve the connectivity of the RMRS if an operator's commands are too aggressive. As illustrated by the experiment above, the aggressive user can neither teleoperate the RMRS nor feel the forces of the other users after breaking the link (1,5). The following section verifies experimentally that the proposed connectivity-preserving passivation strategy can overcome this limitation of P+d control.

B. Teleoperation With Connectivity-Preserving Feedforward–Feedback Passivation Control

Fig. 12 presents the experimental four-user teleoperation of a ten-robot RMRS under the control proposed in this article. The experiment is similar to the one in the previous section (because the users strive to repeat their telemanipulations), but some results are different. In Fig. 12(a), the teleoperated RMRS is more compact, and the couplings between the leader remote robots R1–R4 and their associated local robots L1–L4 are weaker than in Fig. 10(a). This result validates that the proposed controller can maintain the RMRS more tightly interconnected than P+d control, thanks to its connectivity-preserving property. Figs. 12(b) and (c) depict two teleoperator configurations when user 1 strains at $t = 195$ s and relaxes at $t = 196$ s the coupling between their local robot L1 and the leader remote robot R1 in Step 4. They prove that the RMRS behaves analogously under the proposed control and under P+d control: it deforms when user 1 stretches it in Fig. 12(b) and regains its configuration when the user force disappears in Fig. 12(c). Fig. 12(d) shows that the RMRS is more compact and stays farther away from the boundary of the convex hull spanned by the local robots L1–L4 from $t = 208$ s to $t = 217$ s when all users cooperatively transport it to another region in Step 5. This feature can make the proposed passivation controller preferable to P+d control in applications that require the RMRS to cohesively navigate through confined spaces: the users can enforce the safety constraints using their local devices; and the proposed control can maintain the remote robots close to each other and a safe distance away from those constraints. Fig. 12(e) validates the key feature of the proposed controller: its ability to preserve the initial connectivity of the RMRS even when user 1 moves their local robot L1 suddenly with $\Xi = 1.93$ and over a large distance at $t = 255$ s. Step 6 in the experiment demonstrates that the proposed control maintains all connections between the remote robots when user 1 threatens them, by saturating the coupling between the robots L1 and R1 (the red line): the control of the leader remote robots prioritizes their proximity-constrained couplings to other remote robots over their couplings to the associated local robots, which occur over the Internet and are not limited by distances. Favoring connectivity preservation, the proposed passivation controller also preserves the role of all users in the collaborative delivery of the RMRS and in adjusting its spatial distribution after $t = 271$ s [see Fig. 12(f)].

To verify that the proposed feedforward–feedback passivation controller can preserve the tree connectivity of the RMRS, user 1 yanks their local robot L1 repeatedly in Step 6 of the experiment, from $t = 217$ s to $t = 270$ s. Table I lists the aggressiveness Ξ of all the motions of user 1, in chronological order, from left to right and from up to down. The 7th to the 10th and the 16th to the 19th motions of user 1 all have $\Xi \geq 1.78$, namely, they are more rapid and sudden than the motions of user 1 in the first experiment in Section V-A. Nevertheless, they cannot break any communication links of the RMRS. In practical teleoperation, such aggressive manipulations may arise due to human errors and need to be handled appropriately by the teleoperation controller.

Fig. 13 depicts the force feedback $\mathbf{f}_{l1}$ to user 1 and the sum $\mathbf{f}_{h234}$ of all other user-applied forces. As in Fig. 11, the four colored areas correspond to Steps 4–7 in the teleoperation mode, and the seven dots indicate the forces that correspond to the states of the system in Fig. 12. In Step 4, user 1 lifts their local robot L1 9 times from $t = 178$ s to $t = 205$ s. For example, during the motion of L1 from its position in Fig. 12(b) to its position in Fig. 12(c), the force feedback f_{l1}^z changes from -5 N to about 0 N in Fig. 13 to convey to user 1 the displacement of R1 from L1. Then, the RMRS moves from $t = 208$ s to $t = 217$ s in Fig. 12(d), and the volume of the tetrahedron spanned by the local robots decreases, leading to the almost zero feedback forces f_{l1}^x and f_{l1}^z in the pink area of Fig. 13. In Step 6, the repeated aggressive actions of user 1 lead to frequent saturation of the force feedback in the green area of Fig. 13. This figure shows that, at $t = 255$ s, the state of the system in Fig. 12(e) feeds back to user 1 a force $\mathbf{f}_{l1} = (5, -4.5, 5)^\mathsf{T}$ N nearly proportional to the displacement of R1 from L1. After guiding the RMRS to the position in Fig. 12(f), user 1 releases and forces their robot L1 to the bottom and top of its workspace three more times between $t = 277$ s and $t = 285$ s. The force profile is similar to that in Step 4 and implies that the RMRS remains elastic. Notably, the strong agreement of $\mathbf{f}_{l1}$ and $\mathbf{f}_{h234}$ throughout the teleoperation validates that user 1 accurately perceives the sum of all other user forces in steady state, and the sum of all other user forces plus the dynamics of the teleoperator during transient phases.

The experiment confirms that the proposed feedforward–feedback passivation controller has force feedback performance similar to P+d control and can preserve the connectivity of the RMRS in the presence of aggressive user actions.

VI. Conclusion

This article developed a dynamic control strategy for bilateral multiuser teleoperation of an RMRS that guarantees both the tree connectivity of the RMRS and the passivity of the teleoperator. In contrast to existing results, the proposed strategy designs the couplings between the remote robots based on a bounded potential. This design facilitates future extensions to systems

with additional constraints, such as time-delayed communications between, and bounded actuation of, the remote robots. The proposed strategy strictly upper (lower) bounds the energy stored in (passivity level of) the RMRS. To this end, sliding variables at all the remote robots decompose the teleoperator into an interconnection of several subsystems, whose input–output properties inspire a dynamic feedback strategy for passive delay-free teleoperation. Then, a reframing of the overall teleoperator by the "control as interconnection" paradigm leads to a novel feedforward–feedback strategy for passive time-delayed teleoperation. Rigorous proofs claim the performance of the proposed connectivity-preserving passivation strategy in terms of position synchronization, force feedback, and containment control in the steady state. An experimental comparison with P+d control validates the proposed strategy empirically. Future work will augment the control design to address time-delayed communications between the remote robots and physical interactions of the RMRS with the environment and will incorporate intelligence into the RMRS to enable it to execute multiple tasks simultaneously.

REFERENCES

[1] A. Howard, L. E. Parker, and G. S. Sukhatme, "Experiments with a large heterogeneous mobile robot team: Exploration, mapping, deployment and detection," *Int. J. Robot. Res.*, vol. 25, nos. 5/6, pp. 431–447, 2006.

[2] M. Schwager, D. Rus, and J.-J. Slotine, "Decentralized, adaptive coverage control for networked robots," *Int. J. Robot. Res.*, vol. 28, no. 3, pp. 357–375, 2009.

[3] J. Fink, N. Michael, S. Kim, and V. Kumar, "Planning and control for cooperative manipulation and transportation with aerial robots," *Int. J. Robot. Res.*, vol. 30, no. 3, pp. 324–334, 2011.

[4] S. Chung, A. A. Paranjape, P. Dames, S. Shen, and V. Kumar, "A survey on aerial swarm robotics," *IEEE Trans. Robot.*, vol. 34, no. 4, pp. 837–855, Aug. 2018.

[5] A. Franchi, C. Secchi, M. Ryll, H. H. Bülthoff, and P. R. Giordano, "Shared control: Balancing autonomy and human assistance with a group of quadrotor UAVs," *IEEE Robot. Autom. Mag.*, vol. 19, no. 3, pp. 57–68, Sep. 2012.

[6] D. Lee and M. W. Spong, "Bilateral teleoperation of multiple cooperative robots over delayed communication networks: Theory," in *Proc. IEEE Int. Conf. Robot. Autom.*, Apr. 2005, pp. 360–365.

[7] D. Lee, "Semi-autonomous teleoperation of multiple wheeled mobile robots over the Internet," in *Proc. Dyn. Syst. Control Conf.*, 2008, pp. 147–154.

[8] K. Y. Lui, H. Cho, C. Ha, and D. Lee, "First-person view semi-autonomous teleoperation of cooperative wheeled mobile robots with visuo-haptic feedback," *Int. J. Robot. Res.*, vol. 36, nos. 5–7, pp. 840–860, 2017.

[9] E. J. Rodríguez-Seda, J. J. Troy, C. A. Erignac, P. Murray, D. M. Stipanovic, and M. W. Spong, "Bilateral teleoperation of multiple mobile agents: Coordinated motion and collision avoidance," *IEEE Trans. Control Syst. Technol.*, vol. 18, no. 4, pp. 984–992, Jul. 2010.

[10] A. Franchi, C. Secchi, H. I. Son, H. H. Bülthoff, and P. R. Giordano, "Bilateral teleoperation of groups of mobile robots with time-varying topology," *IEEE Trans. Robot.*, vol. 28, no. 5, pp. 1019–1033, Oct. 2012.

[11] C. Secchi, S. Stramigioli, and C. Fantuzzi, "Position drift compensation in port-hamiltonian based telemanipulation," in *Proc. IEEE/RSJ Int. Conf. Intell. Robots Syst.*, 2006, pp. 4211–4216.

[12] D. Lee and D. Xu, "Feedback r-passivity of lagrangian systems for mobile robot teleoperation," in *Proc. IEEE Int. Conf. Robot. Autom.*, May 2011, pp. 2118–2123.

[13] C. Secchi, A. Franchi, H. H. Bülthoff, and P. R. Giordano, "Bilateral teleoperation of a group of UAVs with communication delays and switching topology," in *Proc. IEEE Int. Conf. Robot. Autom.*, May 2012, pp. 4307–4314.

[14] A. Franchi and P. R. Giordano, "Online leader selection for improved collective tracking and formation maintenance," *IEEE Control Netw. Syst.*, vol. 5, no. 1, pp. 3–13, Mar. 2018.

[15] A. Franchi, P. R. Giordano, and G. Michieletto, "Online leader selection for collective tracking and formation control: The second-order case," *IEEE Control Netw. Syst.*, vol. 6, no. 4, pp. 1415–1425, Dec. 2019.

[16] D. Zhou, Z. Wang, and M. Schwager, "Agile coordination and assistive collision avoidance for quadrotor swarms using virtual structures," *IEEE Trans. Robot.*, vol. 34, no. 4, pp. 916–923, Aug. 2018.

[17] A. Franchi, C. Masone, V. Grabe, M. Ryll, H. H. Bülthoff, and P. R. Giordano, "Modeling and control of UAV bearing formations with bilateral high-level steering," *Int. J. Robot. Res.*, vol. 31, no. 12, pp. 1504–1525, 2012.

[18] C. Lin and Y. Liu, "Decentralized estimation and control for bilateral teleoperation of mobile robot network with task abstraction," in *Proc. IEEE Int. Conf. Robot. Autom.*, May 2017, pp. 5384–5391.

[19] L. Sabattini, C. Secchi, B. Capelli, and C. Fantuzzi, "Passivity preserving force scaling for enhanced teleoperation of multirobot systems," *IEEE Robot. Autom. Lett.*, vol. 3, no. 3, pp. 1925–1932, Jul. 2018.

[20] H. Saeidi, J. R. Wagner, and Y. Wang, "A mixed-initiative haptic teleoperation strategy for mobile robotic systems based on bidirectional computational trust analysis," *IEEE Trans. Robot.*, vol. 33, no. 6, pp. 1500–1507, Dec. 2017.

[21] H. Saeidi and Y. Wang, "Incorporating trust and self-confidence analysis in the guidance and control of (SEMI)autonomous mobile robotic systems," *IEEE Robot. Autom. Lett.*, vol. 4, no. 2, pp. 239–246, Apr. 2019.

[22] H. Saeidi, D. G. Mikulski, and Y. Wang, "Trust-based leader selection for bilateral haptic teleoperation of multi-robot systems," in *Proc. IEEE/RSJ Int. Conf. Intell. Robots Syst.*, Sep. 2017, pp. 6575–6581.

[23] S. Sirouspour, "Modeling and control of cooperative teleoperation systems," *IEEE Trans. Robot.*, vol. 21, no. 6, pp. 1220–1225, Dec. 2005.

[24] K. Huang and D. Lee, "Consensus-based peer-to-peer control architecture for multiuser haptic interaction over the internet," *IEEE Trans. Robot.*, vol. 29, no. 2, pp. 417–431, Apr. 2013.

[25] M. Shahbazi, S. F. Atashzar, and R. V. Patel, "A systematic review of multilateral teleoperation systems," *IEEE Trans. Haptics*, vol. 11, no. 3, pp. 338–356, Jul. 2018.

[26] J. Ryu, Q. Ha-Van, and A. Jafari, "Multilateral teleoperation over communication time delay using the time-domain passivity approach," *IEEE Trans. Control Syst. Technol.*, vol. 28, no. 6, pp. 2705–2712, Nov. 2020.

[27] M. Minelli, F. Ferraguti, N. Piccinelli, R. Muradore, and C. Secchi, "An energy-shared two-layer approach for multi-master-multi-slave bilateral teleoperation systems," in *Proc. Int. Conf. Robot. Autom.*, May 2019, pp. 423–429.

[28] L. Sabattini, C. Secchi, M. Cocetti, A. Levratti, and C. Fantuzzi, "Implementation of coordinated complex dynamic behaviors in multirobot systems," *IEEE Trans. Robot.*, vol. 31, no. 4, pp. 1018–1032, Aug. 2015.

[29] W. Ren and Y. Cao, *Distributed Coordination of Multi-Agent Networks: Emergent Problems, Models, and Issues*. New York, NY, USA: Springer, 2010.

[30] M. Ji and M. Egerstedt, "Distributed coordination control of multiagent systems while preserving connectedness," *IEEE Trans. Robot.*, vol. 23, no. 4, pp. 693–703, Aug. 2007.

[31] M. M. Zavlanos and G. J. Pappas, "Distributed connectivity control of mobile networks," *IEEE Trans. Robot.*, vol. 24, no. 6, pp. 1416–1428, Dec. 2008.

[32] R. K. Williams and G. S. Sukhatme, "Constrained interaction and coordination in proximity-limited multiagent systems," *IEEE Trans. Robot.*, vol. 29, no. 4, pp. 930–944, Aug. 2013.

[33] R. K. Williams, A. Gasparri, G. Ulivi, and G. S. Sukhatme, "Generalized topology control for nonholonomic teams with discontinuous interactions," *IEEE Trans. Robot.*, vol. 33, no. 4, pp. 994–1001, Aug. 2017.

[34] M. C. De Gennaro and A. Jadbabaie, "Decentralized control of connectivity for multi-agent systems," in *Proc. 45th IEEE Conf. Decis. Control*, Dec. 2006, pp. 3628–3633.

[35] P. Yang, R. Freeman, G. Gordon, K. Lynch, S. Srinivasa, and R. Sukthankar, "Decentralized estimation and control of graph connectivity for mobile sensor networks," *Automatica*, vol. 46, no. 2, pp. 390–396, 2010.

[36] L. Sabattini, N. Chopra, and C. Secchi, "Decentralized connectivity maintenance for cooperative control of mobile robotic systems," *Int. J. Robot. Res.*, vol. 32, no. 12, pp. 1411–1423, 2013.

[37] L. Sabattini, C. Secchi, N. Chopra, and A. Gasparri, "Distributed control of multirobot systems with global connectivity maintenance," *IEEE Trans. Robot.*, vol. 29, no. 5, pp. 1326–1332, Oct. 2013.

[38] A. Gasparri, L. Sabattini, and G. Ulivi, "Bounded control law for global connectivity maintenance in cooperative multirobot systems," *IEEE Trans. Robot.*, vol. 33, no. 3, pp. 700–717, Jun. 2017.

[39] Z. Kan, E. A. Doucette, and W. E. Dixon, "Distributed connectivity preserving target tracking with random sensing," *IEEE Trans. Autom. Control*, vol. 64, no. 5, pp. 2166–2173, May 2019.
[40] K. Khateri, M. Pourgholi, M. Montazeri, and L. Sabattini, "Decentralized local-global connectivity maintenance for networked robotic teams," *Eur. J. Control*, vol. 51, pp. 110–121, 2020.
[41] A. J. van der Schaft, *L2-Gain and Passivity Techniques in Nonlinear Control*. New York, NY, USA: Springer, 2017.
[42] S. F. Atashzar, I. G. Polushin, and R. V. Patel, "A small-gain approach for nonpassive bilateral telerobotic rehabilitation: Stability analysis and controller synthesis," *IEEE Trans. Robot.*, vol. 33, no. 1, pp. 49–66, Feb. 2017.
[43] S. Hirche and M. Buss, "Human-oriented control for haptic teleoperation," *Proc. IEEE*, vol. 100, no. 3, pp. 623–647, Mar. 2012.
[44] J. E. Colgate and N. Hogan, "Robust control of dynamically interacting systems," *Int. J. Control*, vol. 48, no. 1, pp. 65–88, 1988.
[45] M. Xia, A. Rahnama, S. Wang, and P. J. Antsaklis, "Control design using passivation for stability and performance," *IEEE Trans. Autom. Control*, vol. 63, no. 9, pp. 2987–2993, Sep. 2018.
[46] J. Ryu, D. Kwon, and B. Hannaford, "Stable teleoperation with time-domain passivity control," *IEEE Trans. Robot. Autom.*, vol. 20, no. 2, pp. 365–373, Apr. 2004.
[47] V. Chawda and M. K. O'Malley, "Position synchronization in bilateral teleoperation under time-varying communication delays," *IEEE/ASME Trans. Mechatronics*, vol. 20, no. 1, pp. 245–253, Feb. 2015.
[48] D. Lee and K. Huang, "Passive-set-position-modulation framework for interactive robotic systems," *IEEE Trans. Robot.*, vol. 26, no. 2, pp. 354–369, Apr. 2010.
[49] M. Franken, S. Stramigioli, S. Misra, C. Secchi, and A. Macchelli, "Bilateral telemanipulation with time delays: A two-layer approach combining passivity and transparency," *IEEE Trans. Robot.*, vol. 27, no. 4, pp. 741–756, Aug. 2011.
[50] D. Heck, A. Saccon, R. Beerens, and H. Nijmeijer, "Direct force-reflecting two-layer approach for passive bilateral teleoperation with time delays," *IEEE Trans. Robot.*, vol. 34, no. 1, pp. 194–206, Feb. 2018.
[51] F. Ferraguti *et al.*, "An energy tank-based interactive control architecture for autonomous and teleoperated robotic surgery," *IEEE Trans. Robot.*, vol. 31, no. 5, pp. 1073–1088, Oct. 2015.
[52] E. Nuño, L. Basañez, and R. Ortega, "Passivity-based control for bilateral teleoperation: A tutorial," *Automatica*, vol. 47, no. 3, pp. 485–495, 2011.
[53] R. J. Anderson and M. W. Spong, "Asymptotic stability for force reflecting teleoperators with time delay," *Int. J. Robot. Res.*, vol. 11, no. 2, pp. 135–149, 1992.
[54] G. Niemeyer and J.-J. E. Slotine, "Telemanipulation with time delays," *Int. J. Robot. Res.*, vol. 23, no. 9, pp. 873–890, 2004.
[55] D. Lee and M. W. Spong, "Passive bilateral teleoperation with constant time delay," *IEEE Trans. Robot.*, vol. 22, no. 2, pp. 269–281, Apr. 2006.
[56] E. Nuño, R. Ortega, N. Barabanov, and L. Basañez, "A globally stable PD controller for bilateral teleoperators," *IEEE Trans. Robot.*, vol. 24, no. 3, pp. 753–758, Jun. 2008.
[57] E. Nuño, L. Basañez, R. Ortega, and M. W. Spong, "Position tracking for non-linear teleoperators with variable time delay," *Int. J. Robot. Res.*, vol. 28, no. 7, pp. 895–910, 2009.
[58] C. Hua and X. P. Liu, "Delay-dependent stability criteria of teleoperation systems with asymmetric time-varying delays," *IEEE Trans. Robot.*, vol. 26, no. 5, pp. 925–932, Oct. 2010.
[59] N. Chopra, M. W. Spong, and R. Lozano, "Synchronization of bilateral teleoperators with time delay," *Automatica*, vol. 44, no. 8, pp. 2142–2148, 2008.
[60] E. Nuño, R. Ortega, and L. Basañez, "An adaptive controller for nonlinear teleoperators," *Automatica*, vol. 46, no. 1, pp. 155–159, 2010.
[61] Y. Liu and N. Chopra, "Control of semi-autonomous teleoperation system with time delays," *Automatica*, vol. 49, no. 6, pp. 1553–1565, 2013.
[62] K. J. Kuchenbecker and G. Niemeyer, "Modeling induced master motion in force-reflecting teleoperation," in *Proc. IEEE Int. Conf. Robot. Autom.*, Apr. 2005, pp. 348–353.
[63] P. Robuffo Giordano, A. Franchi, C. Secchi, and H. H. Bülthoff, "A passivity-based decentralized strategy for generalized connectivity maintenance," *Int. J. Robot. Res.*, vol. 32, no. 3, pp. 299–323, 2013.
[64] C. Secchi, A. Franchi, H. H. Bülthoff, and P. R. Giordano, "Bilateral control of the degree of connectivity in multiple mobile-robot teleoperation," in *Proc. IEEE Int. Conf. Robot. Autom.*, May 2013, pp. 3645–3652.
[65] D. Lee, A. Franchi, H. I. Son, C. Ha, H. H. Bülthoff, and P. R. Giordano, "Semiautonomous haptic teleoperation control architecture of multiple unmanned aerial vehicles," *IEEE/ASME Trans. Mechatronics*, vol. 18, no. 4, pp. 1334–1345, Aug. 2013.
[66] M. Mesbahi and M. Egerstedt, *Graph Theoretic Methods in Multiagent Networks*. Princeton, NJ, USA: Princeton Univ. Press, 2010.
[67] Y. Yang, D. Constantinescu, and Y. Shi, *Passive multi-user teleoperation of a multi-robot system with connectivity-preserving containment*. Accessed: Jun. 15, 2021. [Online]. Available: https://drive.google.com/file/d/15QAhbqun0PyVPZeDfxdoTTzzVgyDlmaK/view?usp=sharing
[68] Y. Yang, D. Constantinescu, and Y. Shi, "Connectivity-preserving swarm teleoperation with a tree network," in *Proc. IEEE/RSJ Int. Conf. Intell. Robots Syst.*, Nov. 2019, pp. 3624–3629.
[69] M. Laghi, A. Ajoudani, M. G. Catalano, and A. Bicchi, "Unifying bilateral teleoperation and tele-impedance for enhanced user experience," *Int. J. Robot. Res.*, vol. 39, no. 4, pp. 514–539, 2020.
[70] M. Panzirsch, H. Singh, and C. Ott, "The 6-DoF implementation of the energy-reflection based time domain passivity approach with preservation of physical coupling behavior," *IEEE Robot. Autom. Lett.*, vol. 5, no. 4, pp. 6756–6763, Oct. 2020.

Yuan Yang (Member, IEEE) received the B.Eng. degree in mechanical design, manufacturing and automation from the Harbin Institute of Technology, Harbin, China, in 2015, and the M.A.Sc. and Ph.D. degrees in mechanical engineering from the University of Victoria, Victoria, BC, Canada, in 2017 and 2021, respectively.

He is currently a Postdoctoral Fellow with the Department of Electrical Engineering, Polytechnique Montréal, Montréal, QC, Canada. His current research interests include passivity-based control, distributed optimization, and reinforcement learning, with applications to human–robot teams.

Daniela Constantinescu (Member, IEEE) received the Ph.D. degree in electrical and computer engineering from the University of British Columbia, Vancouver, BC, Canada, in 2005.

Since 2005, she has been with the University of Victoria, Victoria, BC, where she is currently an Associate Professor with the Department of Mechanical Engineering. Her current research interests include teleoperation and haptic systems, distributed control for network robotic systems, human–robot interaction, robotics, and dynamics.

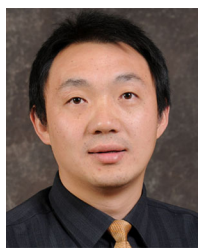

Yang Shi (Fellow, IEEE) received the Ph.D. degree in electrical and computer engineering from the University of Alberta, Edmonton, AB, Canada, in 2005.

From 2005 to 2009, he was with the University of Saskatchewan, Saskatoon, SK, Canada. He is currently a Professor with the Department of Mechanical Engineering, University of Victoria, Victoria, BC, Canada. His current research interests include networked and distributed systems, model-predictive control, cyber-physical systems, robotics and mechatronics, autonomous intelligent systems (autonomous underwater vehicles and unmanned aerial vehicles), and energy system applications.

Dr. Shi is a Fellow of the American Society of Mechanical Engineers, the Canadian Society of Mechanical Engineers, and the Engineering Institute of Canada. He is a registered Professional Engineer in British Columbia, Canada.